

## Discovery of Peptidomimetic Antibody-Drug Conjugate Linkers with Enhanced Protease Specificity

Binqing Wei, Janet Gunzner-Toste, Hui Yao, Tao Wang, Jing Wang, Zijin Xu, Jinhua Chen, John Wai, Jim Nonomiya, Siao Ping Tsai, Josefa dela Cruz-Chuh, Katherine Ruth Kozak, Yichin Liu, Shang-Fan Yu, Jeff Lau, Guangmin Li, Gail D. Lewis Phillips, Doug Leipold, Amrita Kamath, Dian Su, Keyang Xu, Charles Eigenbrot, Stefan Steinbacher, Rachana Ohri, Helga Raab, Leanna R. Staben, Guiling Zhao, John A. Flygare, Thomas H Pillow, Vishal Verma, and Brian Salvatore Safina  
*J. Med. Chem.*, **Just Accepted Manuscript** • DOI: 10.1021/acs.jmedchem.7b01430 • Publication Date (Web): 11 Dec 2017

Downloaded from <http://pubs.acs.org> on December 12, 2017

### Just Accepted

“Just Accepted” manuscripts have been peer-reviewed and accepted for publication. They are posted online prior to technical editing, formatting for publication and author proofing. The American Chemical Society provides “Just Accepted” as a free service to the research community to expedite the dissemination of scientific material as soon as possible after acceptance. “Just Accepted” manuscripts appear in full in PDF format accompanied by an HTML abstract. “Just Accepted” manuscripts have been fully peer reviewed, but should not be considered the official version of record. They are accessible to all readers and citable by the Digital Object Identifier (DOI®). “Just Accepted” is an optional service offered to authors. Therefore, the “Just Accepted” Web site may not include all articles that will be published in the journal. After a manuscript is technically edited and formatted, it will be removed from the “Just Accepted” Web site and published as an ASAP article. Note that technical editing may introduce minor changes to the manuscript text and/or graphics which could affect content, and all legal disclaimers and ethical guidelines that apply to the journal pertain. ACS cannot be held responsible for errors or consequences arising from the use of information contained in these “Just Accepted” manuscripts.

# Discovery of Peptidomimetic Antibody-Drug Conjugate Linkers with Enhanced Protease Specificity

BinQing Wei,<sup>\*,†</sup> Janet Gunzner-Toste,<sup>†</sup> Hui Yao,<sup>‡</sup> Tao Wang,<sup>‡</sup> Jing Wang,<sup>‡</sup> Zijin Xu,<sup>‡</sup> Jinhua Chen,<sup>‡</sup> John Wai,<sup>‡</sup> Jim Nonomiya,<sup>†</sup> Siao Ping Tsai,<sup>†</sup> Josefa Chuh,<sup>†</sup> Katherine R. Kozak,<sup>†</sup> Yichin Liu,<sup>†</sup> Shang-Fan Yu,<sup>†</sup> Jeff Lau,<sup>†</sup> Guangmin Li,<sup>†</sup> Gail D. Phillips,<sup>†</sup> Doug Leipold,<sup>†</sup> Amrita Kamath,<sup>†</sup> Dian Su,<sup>†</sup> Keyang Xu,<sup>†</sup> Charles Eigenbrot,<sup>†</sup> Stefan Steinbacher,<sup>§</sup> Rachana Ohri,<sup>†</sup> Helga Raab,<sup>†</sup> Leanna R Staben,<sup>†</sup> Guiling Zhao,<sup>†</sup> John A. Flygare,<sup>†</sup> Thomas H. Pillow,<sup>†</sup> Vishal Verma,<sup>†</sup> Brian Safina<sup>\*,†</sup>

<sup>†</sup>Genentech, Inc., 1 DNA Way, South San Francisco, CA 94080, USA

<sup>‡</sup>WuXi AppTec, 288 Fute Zhong Road, Waigaoqiao Free Trade Zone, Shanghai, 200131, China

<sup>§</sup>Proteros Biostructures GmbH, Bunsenstr. 7a, D-82152 Martinsried, Germany

\* Correspondence: Wei.BinQing@gene.com , Safina.Brian@gene.com

## ABSTRACT

Antibody-Drug Conjugates (ADCs) have become an important therapeutic modality for oncology, with three approved by the FDA and over 60 others in clinical trials. Despite the progress, improvements in ADC therapeutic index are desired. Peptide-based ADC linkers that are cleaved by lysosomal proteases have shown sufficient stability in serum, and effective payload-release in targeted cells. If the linker can be preferentially hydrolyzed by tumor-specific proteases, safety margin may improve. However, the use of peptide-based linkers limits our ability to modulate protease specificity. Here we report the structure-guided discovery of novel, non-peptidic ADC linkers. We show that a cyclobutane-1,1-dicarboxamide-containing linker is hydrolyzed predominantly by cathepsin B while the

1 valine-citrulline dipeptide linker is not. ADCs bearing the non-peptidic linker are as efficacious and  
2 stable in vivo as those with the dipeptide linker. Our results strongly support the application of the  
3 peptidomimetic linker and present new opportunities for improving the selectivity of ADCs.  
4  
5  
6  
7

## 8 **Introduction**

9  
10 The use of antibody drug conjugates has emerged as a powerful approach to deliver cytotoxic  
11 drugs to tumor cells. There are a number of clinical trials ongoing involving this class of therapeutics.<sup>1</sup>  
12 However, the therapeutic window of existing clinical-stage ADC's is relatively narrow.<sup>2,3</sup> Factors likely  
13 contributing to this phenomenon include linker instability that results in premature release of the  
14 attached cytotoxic payload during systemic circulation,<sup>4,5</sup> and the release of payload in non-cancerous  
15 tissues due to non-specific uptake (pinocytosis) and/or low level of antigen-expression on normal cells.<sup>6</sup>  
16 Accordingly, current approaches to the design of new ADCs seek to improve on at least one of these  
17 parameters in order to achieve enhanced clinical performance.<sup>7</sup>  
18  
19  
20  
21  
22  
23  
24  
25  
26  
27  
28

29 The use of protease-cleavable peptide linkers, in particular a valine-citrulline dipeptide linker  
30 (Val-Cit),<sup>8</sup> has proved to be an effective strategy for ADC construction owing much to the clinical  
31 success of brentuximab vedotin.<sup>9</sup> Peptidic linkers have been shown to be stable in circulation and able  
32 to effectively release attached payloads inside target cells<sup>10</sup> and, when conjugated to noninternalizing  
33 antibodies, outside target cells.<sup>11</sup> They are the subject of active investigations.<sup>12,13</sup> It is generally  
34 believed that lysosomal cathepsin B is one of the proteases mainly responsible for the cleavage of the  
35 Val-Cit ADC linker inside target cells. Other proteases, including both close homologs of cathepsin B  
36 (e.g. cathepsin X) as well as enzymes that are distantly related/unrelated (e.g. cathepsins L and D), may  
37 also be involved.<sup>8</sup> Importantly, the precise extent to which the activation of Val-Cit ADC linker  
38 depends on cathepsin B enzyme activity has not been reported.  
39  
40  
41  
42  
43  
44  
45  
46  
47  
48  
49  
50

51 Cathepsin B (EC 3.4.22.1) is a member of the papain family of cysteine proteases.<sup>14</sup> It can  
52 function as an exopeptidase (i.e. carboxydipeptidase) at acidic pH as well as an endopeptidase at neutral  
53 pH, owing to a structural feature called the occluding loop.<sup>15,16</sup> Cathepsin B is normally associated with  
54  
55  
56  
57  
58  
59  
60

lysosomes involved in autophagy and immune response, but numerous studies have shown that its overexpression is correlated with invasive and metastatic phenotypes in cancers.<sup>17,18</sup> A major mechanism that cathepsin B contributes to cancer progression is its involvement in degradation of the extracellular matrix.<sup>19</sup> A recent report suggested that the exopeptidase and endopeptidase activities of cathepsin B both contribute to the proteolysis of extracellular matrix and tumor cell invasion.<sup>20</sup> Therefore it is conceivable that, compared to the Val-Cit linker, an ADC linker whose hydrolysis is more dependent on cathepsin B may help target the release of the attached cytotoxic payloads more specifically to tumor cells.

In an effort to further enhance the tumor-specific release of ADC payload via protease-dependent cleavage, we sought to identify non-peptidic protease-substrates that could serve as effective linkers for ADC. To the best of our knowledge, the exploration of such peptidomimetic ADC linkers has not been previously reported. We anticipated that, due to a reduction in the number of hydrolysable amide bonds, the new linker moieties would offer greater opportunities to modulate the recognition by tumor-specific/elevated proteases relative to the legacy peptide linkers. In this initial report, we describe the identification of several peptidomimetic linkers with enhanced specificity toward cathepsin B that efficiently release various attached payloads following intracellular ADC-mediated delivery.

## Results and Discussion

To facilitate rapid in vitro biochemical testing of our new linker designs, we devised a simplified molecular construct to assess the ability of various linker-payloads to undergo protease-mediated cleavage (Scheme 1, compound **1**). Using this system, hydrolysis of the aniline-derived amide bond present in **1** can be readily detected through a norfloxacin payload released by subsequent immolation of the liberated *p*-aminobenzylcarbonyl moiety. We anticipated that these simple molecules could be used to model the ability of peptidomimetic linkers to undergo similar protease-effected cleavage following ADC-mediated intracellular delivery. We expect the model to be valid regardless of whether the linker-payload is attached to an antibody or to just a cysteine, since the exact sequence of events between

linker cleavage and antibody degradation is not known.

To validate our approach of using this simplified molecular construct, we applied it to some representative dipeptide linkers and measured their cleavage kinetic parameters using a constant concentration of cathepsin B enzyme. Michaelis-Menten steady-state  $V_{\max}$  and  $K_m$  data for the linkers were compared as the P1 and P2 side chains with different charge, polarity and shape were explored (Scheme 1, Table 1). A hydrogen bond donor-rich citrulline sidechain at the P1 position afforded a ~9 fold higher  $V_{\max}$  value than an alanine sidechain (**1** vs. **2**). A positively charged arginine sidechain at this position further improved substrate binding affinity (>10 fold reduction of  $K_m$ ) compared to the citrulline, making **3** the most preferred substrate in the biochemical assay. Despite its positive charge,  $\beta$ -(4-piperidinyl) alanine (**4**) caused a ~10 fold decrease in binding affinity than **3**, suggesting that this bulky sidechain may fit less well in the active site. At the P2 position, bulky aromatic sidechains gained affinity (lower  $K_m$ ) at the cost of  $V_{\max}$ , resulting in no improvement in the ratio of  $V_{\max}/K_m$  ratio (**1** vs. **5** or **6**). These observed trends are consistent with previous reports of the substrate preference profile of human cathepsin B determined using combinatorial peptide libraries,<sup>21,22</sup> and support the use of this approach. Additionally it is important to note that, despite having a  $V_{\max}/K_m$  value 3-fold lower than the Val-Cit linker, the valine-alanine linker (Val-Ala) has been successfully used in ADCs currently in clinical trials.<sup>10</sup> Therefore we reasoned that a proteolytic efficiency level similar to that of the Val-Ala linker would be sufficient for an effective ADC.

To guide the design of new, non-peptidic linkers cleavable by cathepsin B, we identified the structure of the enzyme bound to a dipeptidyl nitrile inhibitor (PDB entry 1GMY).<sup>23</sup> This structure was particularly informative of the substrate recognition by the enzyme because the inhibitor has a peptide scaffold while its nitrile moiety formed a thioimidate ester with the catalytic cysteine residue (Cys29), mimicking the acyl enzyme intermediate of substrate hydrolysis (Figure 1A and 1B).<sup>23</sup> The amide backbone of the molecule extends along the active site, forming hydrogen bonds with Gly74 and Gly198 residues known to be critical for substrate binding (Figure 1B).<sup>23</sup> At the position corresponding to the P1 residue of peptide substrate is a glycine moiety. Its C $\alpha$  carbon atom is within 5 Å of the

1 carboxylate group of Glu122 residue, which has been proposed to confer a preference for cationic  
2 sidechains at P1 position.<sup>15,23</sup> At the position corresponding to the P2 residue is a phenylalanine-like  
3 moiety, fitting snugly in a hydrophobic pocket presumably occupied by those lipophilic sidechains  
4 favored at this position (e.g. valine and phenylalanine). We hypothesized that these backbone and  
5 sidechain interactions together hold the scissile amide bond in the correct position for nucleophilic  
6 attack by Cys29. This led us to investigate two ways to design non-peptidic substrates: (1) to replace  
7 the amide bond between the P1 and P2 residues, and (2) to replace the P2 residue.  
8  
9  
10  
11  
12  
13  
14  
15

16 We first sought to replace the amide moiety between the P1 and P2 residues while maintaining  
17 the interaction of those sidechains with the protein. Guided by modeling based on the crystal structure  
18 (Figure 1B, Supporting Information Figures S1A and S1B), we identified two chemical series that  
19 showed significant activities as substrate: fluoro olefins (Table 2) and 1,2,3-triazoles (Table 3). With a  
20 citrulline sidechain at the P1 position, the valine-fluoroolefin-citrulline linker (**7**) showed a 6-fold lower  
21  $V_{\max}$  value and a 7-fold higher  $K_m$  value than the Val-Cit peptide linker (**1**), amounting to a nearly 40-  
22 fold reduction in the  $V_{\max}/K_m$  ratio. Changing the P1 sidechain from citrulline to alanine decreased the  
23 catalytic efficiency by approximately 6 fold (**7** vs. **8**), which is consistent with the trend observed from  
24 the corresponding peptide linkers (**1** vs. **2**). In the triazole series, the valine-triazole-citrulline linker (**9**)  
25 showed a 210-fold loss in catalytic efficiency relative to the Val-Cit linker. Replacing the citrulline  
26 sidechain with an arginine (**10**) or a lysine (**11**) sidechain at the P1 position improved the cleavage  
27 efficiency of the triazole linker by 18 to 29 fold, though the substrates were still significantly less active  
28 than the corresponding peptide linkers (**10** vs. **3**). Unlike the peptide linkers, incorporation of an  
29 aromatic P2 sidechain reduced the cleavage efficiency (**11** vs. **12**, and **9** vs. **13**). Based on modeling, we  
30 had anticipated that for both these series, some of the hydrogen bonds between the linker's peptide  
31 backbone and the protein could be lost (Supporting Information Figure S1A and S1B). The reduction in  
32 proteolytic efficiency of those new molecules relative to the peptides suggested to us that those  
33 hydrogen bond interactions are critical.  
34  
35  
36  
37  
38  
39  
40  
41  
42  
43  
44  
45  
46  
47  
48  
49  
50  
51  
52  
53  
54  
55  
56

57 Next we sought to replace the P2 amino acid of peptide linker while keeping its hydrogen bond  
58  
59  
60

1 interactions with the residues Gly74 and Gly198 of the protease. Using a computational, shape-  
2 similarity search, we identified the cyclobutane-1,1-dicarboxamide series (“cBu”, Figure 1A, 1C and  
3 1D). The cyclobutyl group was predicted to be optimal in size to fill the hydrophobic S2 pocket, while  
4 the 1,1-dicarboxamide moiety was expected to form all three hydrogen bonds to the protein like the  
5 peptide linker. Furthermore, the bound conformation of cyclobutane-1,1-dicarboxamide predicted by  
6 modeling was found energetically favored. We tested those predictions by making a series of  
7 compounds, varying the moieties on either side of the cyclobutyl ring as well as the ring itself (Table 4).  
8 As the ring size ranged from 3 to 6 atoms, the  $V_{\max}$  and  $V_{\max}/K_m$  ratio both peaked when the size  
9 reached 4 (compounds **14-17**). The linker bearing a *gem*-dimethyl glycine (**18**) showed an activity too  
10 low to be determined under our assay conditions. At the P1 position, compared to a citrulline sidechain  
11 (**15**), an arginine sidechain increased the cleavage efficiency of the linker by about 8 fold (**19**), while a  
12 lysine or dimethyl lysine sidechain only improved the  $V_{\max}/K_m$  ratio by up to about 3 fold (**20, 21**).  
13 Acetylation of the lysine sidechain reduced the  $V_{\max}/K_m$  ratio by about 2 fold (**22**). More significantly,  
14 removal of all hydrogen bond donors at this position rendered the cleavage activity too low to be  
15 determined (**23**). In addition to the P1 and P2 positions, we also explored substitutions on the cBu  
16 linker that correspond to the P3 sidechain of the peptide linker. Modeling suggested that an  
17 aryl/heteroaryl ring with appropriate chirality may contribute to tighter binding affinity by stacking with  
18 the backbone amide of Gly74 and interacting with Try75 residue. Indeed, compared to an isopropyl  
19 group (**24**), a 3-thiophenyl (**25**) or phenyl (**27**) moiety increased the  $V_{\max}/K_m$  ratio by 5-10 fold. That  
20 improvement was more due to tighter substrate-binding than better  $V_{\max}$ . Given that both Val-Cit and  
21 Val-Ala dipeptides were shown effective linkers *in vivo*, it was not clear to us that a P3 substitution  
22 maybe necessary, so we did not try to optimize the P3 moiety further.

23 To verify our computational model of the cBu linker, we obtained a crystal structure of human  
24 cathepsin B in complex with an analog of the cBu-Cit compound (Table 4, **28**). Because **15** would be  
25 hydrolyzed by the enzyme, we replaced the scissile amide bond with an electrophilic cyano group to  
26 trap the hydrolysis product. The resulting 1.6 Å-resolution crystallographic structure showed **28**

1 forming a thioimidate ester with the catalytic residue Cys29 (Figure 1D and 1E), like the PDB structure  
2 that guided the modeling (Figure 1A). Gratifyingly, some of the predicted interactions were observed:  
3 the dicarboxamide moiety is well-positioned to form three hydrogen bonds with residues Gly74 and  
4 Gly198, and the cyclobutyl ring indeed occupies the S2 pocket. The electron density was sufficient to  
5 determine the coordinates of the citrulline side chain only up to the C<sub>β</sub> atom. We speculated that, in the  
6 absence of a substrate leaving group, the rest of the side chain could be rather mobile. Also, there was  
7 not enough electron density to define the position of the terminal methyl or the chirality of **28**. Overall,  
8 the crystallographic structure as well as the data (Table 4) confirmed our computational model for the  
9 cBu linker.  
10  
11  
12  
13  
14  
15  
16  
17  
18  
19

20  
21 Among the new peptidomimetic linkers we identified,  $V_{\max}$  values for the cBu series were found  
22 to be similar to those for the peptide linkers while the fluoroolefin and the triazole series exhibited lower  
23  $V_{\max}$  values (Figure 2). In terms of  $V_{\max}/K_m$  ratio, the cBu linker was about 15 fold lower than the  
24 corresponding peptide linker (**15** vs. **1**, **19** vs. **3**). We wondered whether/how this difference would  
25 affect the payload release and efficacy of ADC.  
26  
27  
28  
29  
30  
31

32 Using those new, non-peptidic linkers, we prepared ADCs conjugated to different payloads  
33 (Tables 5 and 6). We adopted a cysteine-engineering strategy that allows for the straightforward  
34 conjugation of payloads to yield homogeneous antibody-drug conjugates.<sup>24</sup> The drug/antibody ratios  
35 (DAR) for all the conjugates were between 1.8 and 2 as determined by LC/MS analysis of the lysyl  
36 endopeptidase digest of the ADCs. Here we report the data from ADCs conjugated at position 118 (EU  
37 numbering) on the antibody heavy chain. The results are representative of our findings using ADCs  
38 conjugated at different sites<sup>25</sup> (data not shown). Figure 3A shows a representative data set obtained with  
39 ADCs carrying monomethyl auristatin E<sup>26</sup> (MMAE) payload. In the Her2-overexpressing SK-BR-3  
40 cells, anti-Her2 ADCs using either Val-Cit (**29**) or cBu-Cit (**31**) linkers were equally active in inhibiting  
41 cell proliferation. As expected, a non-target control antibody (anti-CD22) conjugated with MMAE  
42 using the cBu-Cit linker had little activity in SK-BR-3 cells. Similarly, the anti-Her2 ADCs showed  
43 very small effects against MCF7 cells which express only low levels of the Her2 antigen (data not  
44  
45  
46  
47  
48  
49  
50  
51  
52  
53  
54  
55  
56  
57  
58  
59  
60

1 shown). Collectively, the data indicated that the two ADCs were equally active in inhibiting the  
2 proliferation of the cancer cells and their activities were antigen-specific. However, this equivalence in  
3 activity does not necessarily mean that the rates of payload release inside target cells are similar for the  
4 two linkers. This is because, for example, full release of free MMAE molecules may not be required for  
5 the activity.  
6  
7  
8  
9  
10

11 Given the differences in  $V_{\max}$  and  $K_m$  values observed for the Val-Cit and cBu-Cit model  
12 constructs (**1** vs **15**), we wondered whether the two ADCs (**29** vs. **31**) may differ in their ability to  
13 release free MMAE in targeted cells. We measured the concentrations of MMAE inside SK-BR-3 cells  
14 after ADC treatment. A duration of 23 hours was found optimal for the assay as it was long enough to  
15 allow ADCs to be substantially endocytosed and extensive cell killings or lysis had not started yet. We  
16 tested ADC concentrations ranging from 0.08 to 10  $\mu\text{g/mL}$  and found that the Her2-mediated  
17 endocytosis appeared to saturate at about the 2  $\mu\text{g/mL}$  level. Surprisingly, no statistically significant  
18 difference in the amounts of released MMAE was found between an ADC containing the cBu-Val linker  
19 (**31**) or one bearing the Val-Cit peptide linker (**29**, Figure 3B). This was observed at all ADC  
20 concentrations tested regardless of whether the target-mediated endocytosis reached saturation or not.  
21 To test whether enzymatic or non-enzymatic process underlie the release of MMAE, two ADCs  
22 containing the respective (R)-citrulline linkers (**30**, **32**) were included for comparison. Switching from  
23 the S- to the R-citrulline is expected to render those linkers resistant to proteases. Indeed, both **30** and  
24 **32** afforded negligible release of MMAE at all concentration levels examined. This confirms that the  
25 observed release resulted from protease hydrolysis instead of non-enzymatic process. The apparent  
26 discrepancy between these observations in the cells and the  $V_{\max}/K_m$  data of the corresponding model  
27 compounds (**1** vs. **15**) can be explained by the fact that the cathepsin B assay does not fully capture how  
28 the ADC linkers are degraded in cell lysosome. For example, intracellular concentrations of the  
29 substrates (i.e. ADC) and/or the proteases may be substantially different (higher) than those in the  
30 enzymatic assay. In addition, other proteases besides cathepsin B may contribute to intracellular payload  
31 release. To further probe this latter possibility, we conducted additional experiments using the MMAE  
32  
33  
34  
35  
36  
37  
38  
39  
40  
41  
42  
43  
44  
45  
46  
47  
48  
49  
50  
51  
52  
53  
54  
55  
56  
57  
58  
59  
60

1 conjugates.

2  
3 Using a panel of commercially available protease inhibitors with varying degrees of specificity,  
4 we assessed the impact of these reagents on the MMAE payload release from several ADCs bearing  
5 peptide or non-peptidic linkers (**29**, **31**, **33**, **34**, Figure 4). We tested CA-074\_Me<sup>27</sup> (cathepsin B  
6 inhibitor), CAA0225<sup>28</sup> (cathepsin L inhibitor), BML\_244<sup>29</sup> (cathepsin K inhibitor), pepstatin<sup>30</sup> (inhibitor  
7 of aspartyl proteases such as cathepsin D), and leupeptin<sup>31</sup> (inhibitor of cysteine, serine and threonine  
8 proteases). The inhibitors were applied at a concentration of 50μM in order to saturate the enzymes.  
9  
10 Interestingly, release of MMAE from the Val-Cit-containing ADC (**29**) appeared resistant to all but the  
11 broad-spectrum protease inhibitor leupeptin, which reduced the intracellular MMAE level by 50%. For  
12 example, only a 15%-decrease in the MMAE level was observed upon the treatment with either the  
13 aspartyl proteases inhibitor (not statistically significant) or the potent cathepsin B inhibitor. In contrast,  
14 for the three ADCs bearing the peptidomimetic linkers, the release of MMAE was over 90% blocked by  
15 leupeptin. More importantly, the payload release of those ADCs was more sensitive to the inhibition of  
16 cathepsin B than that of the Val-Cit-containing ADC. For the cBu-Cit-containing ADC (**31**), the  
17 MMAE release was over 75% suppressed while, for the triazole (**34**) and the fluoroolefin-containing  
18 ADCs (**33**), the reductions were 60% and 32%, respectively. The additional decrease of MMAE level  
19 upon the treatment with leupeptin compared to that with the cathepsin B inhibitor suggest that some  
20 other enzyme(s) may contribute to the cleavage of these nonpeptidic linkers as well. We also observed  
21 a 26% decrease in payload release by the triazole-containing ADC after the treatment with the cathepsin  
22 L-specific inhibitor. It is important to note that this comparison relies on the published specificity data  
23 of those inhibitors. Nevertheless, the observed differences strongly suggest that the new  
24 peptidomimetic linkers, especially cBu-Cit linker, have an enhanced protease specificity toward  
25 cathepsin B compared to the Val-Cit peptide linker.  
26  
27  
28  
29  
30  
31  
32  
33  
34  
35  
36  
37  
38  
39  
40  
41  
42  
43  
44  
45  
46  
47  
48  
49  
50  
51

52  
53 We next compared CD22-targeting ADCs bearing the cBu-Cit (**31**) or Val-Cit linker (**29**) in their  
54 efficacy and stability in mouse xenograft tumor models. In a CD22-expressing lymphoma model  
55 (WSU-DLCL2), the two ADCs displayed equivalent, target-dependent activity when administered at  
56  
57  
58  
59  
60

1 two different doses (Figure 5A). No body weight loss was observed from either conjugate at up to 8  
2 mg/kg dose level suggesting they were both well-tolerated (Supporting Information, Figure S2). We  
3 also tested the same ADCs in another CD22-expressing lymphoma model (Bjab-luc), and again  
4 observed equivalent efficacies for the two conjugates (Figure 5B). To see if this observation was only  
5 applicable to tubulin-targeting payloads, we also tested a DNA-damaging payload,  
6 pyrrolbenzodiazepine-dimer<sup>32</sup> (PBD) (Table 6). In a Napi2b-expressing ovarian cancer model  
7 (OVCAR3X2.1), Napi2b-targeting ADCs containing either the Val-Cit or cBu-Cit linkers were both  
8 efficacious in inhibiting tumor growth when dosed at the 3 mg/kg level (Figure 5C). Interestingly, the  
9 cBu-Cit linked ADC appeared somewhat more potent and afforded tumor regression in this model. The  
10 efficacy comparison suggested that, in the tumor cells, the proteolytic capacity of cathepsin B was  
11 sufficient for effective release of payload from the cBu-Cit linker. Contributions by other proteases that  
12 can digest the Val-Cit but not the cBu-Cit linker are not required for the efficacy. Besides the efficacy,  
13 we also monitored the pharmacokinetic profiles of the two ADCs in the same mouse xenograft study.  
14 For example, for the 1mg/kg dose groups in the above Bjab-luc lymphoma study (Figure 5B, group 2  
15 and 4), no significant difference was observed in either the half-life of the antibody (Figure 6A) or the  
16 stability of the conjugate (Figure 6B) between the two ADCs bearing different linkers. This equivalence  
17 in both antibody half-life and conjugate stability between the Val-Cit and the cBu-Cit linkers was also  
18 demonstrated in mouse tumor studies using ADCs carrying the PBD payload (data not shown).  
19  
20  
21  
22  
23  
24  
25  
26  
27  
28  
29  
30  
31  
32  
33  
34  
35  
36  
37  
38  
39  
40  
41  
42

## 43 **Conclusion**

44  
45 Structure-based design led to the discovery of three series of non-peptidic ADC linkers,  
46 including the cBu series which exhibited a level of proteolysis efficiency approaching that of the peptide  
47 linkers. A crystal structure of an analogous covalent inhibitor bound to cathepsin B confirmed the  
48 modeling predictions regarding how a cBu-Cit linker is recognized by the protease active site for  
49 cleavage. A comparison of the cBu-Cit linker with the Val-Cit linker in cancer cell lines found that they  
50 exhibited equally potent anti-proliferation effects and displayed similar rates of intracellular payload-  
51  
52  
53  
54  
55  
56  
57  
58  
59  
60

1 release. Using selected protease inhibitors, we showed that the cleavage of the cBu-Cit linker  
2 predominantly depends on cathepsin B. In contrast, the degradation of the Val-Cit peptide linker was  
3 resistant to the inhibition of cathepsin B. Furthermore, ADCs containing the cBu-Cit linker were  
4  
5 resistant to the inhibition of cathepsin B. Furthermore, ADCs containing the cBu-Cit linker were  
6  
7 equally efficacious and stable in multiple mouse tumor models compared to the conjugates bearing the  
8  
9 Val-Cit linker. This equivalence in in vivo efficacy and stability was consistently observed with ADCs  
10  
11 delivering MMAE drug (a tubulin polymerization blocker) as well as ADCs carrying PBD dimer  
12  
13 payload (a DNA-alkylator). Our data support the application of the new peptidomimetic linkers in the  
14  
15 construction of ADC therapeutics, and demonstrate the feasibility and opportunity to tailor the linker  
16  
17 moiety toward cleavage by tumor-specific/enhanced proteases.  
18  
19  
20  
21  
22

## 23 **Experimental Section**

24  
25  
26 **Cathepsin B cleavage assay** Cathepsin B-catalyzed linker cleavage activity was assessed by an  
27  
28 LC/MS, MRM-based quantitation method. Briefly, varying concentrations of experimental linker (1.5-  
29  
30 fold serial dilution from 100  $\mu$ M maximum down to 1.16  $\mu$ M minimum) were incubated with 2 nM  
31  
32 human liver Cathepsin B (EMD Millipore, #219364), 25 nM Norfloxacin-d<sub>5</sub> internal standard (CDN  
33  
34 Isotopes, #D-7196), 10 mM MES pH 6.0, and 1 mM DTT. The reaction was incubated for 1 hour at  
35  
36 37°C, followed by quenching with the addition of an equal volume of 2% formic acid in water. Free  
37  
38 Norfloxacin liberated by Cathepsin B and Norfloxacin-d<sub>5</sub> internal standard were quantitated by an  
39  
40 LC/MS MRM method on a Sciex 5500 QTRAP mass spectrometer (Sciex, Framingham, MA) equipped  
41  
42 with a Waters Acquity H-class uHPLC. Norfloxacin and Norfloxacin-d<sub>5</sub> were purified and desalted  
43  
44 using a Water BEH-C18 column, using a gradient of water/acetonitrile with 0.1% formic acid.  
45  
46 Measured Norfloxacin MRM AUC was normalized against Norfloxacin-d<sub>5</sub> AUC, then plotted against  
47  
48 linker concentration using GraphPad Prism (GraphPad Software, La Jolla, CA). The resulting data was  
49  
50 fitted for  $K_m$  and  $V_{max}$  values using Michaelis-Menten equation. Each experiment was done in duplicate  
51  
52  
53  
54  
55  
56  
57  
58  
59  
60

1 for each linker concentration. MRM parameters for Norfloxacin: Q1=320, Q3=233.1, collision  
2 energy=30; MRM parameters for Norfloxacin-d<sub>5</sub>: Q1=325, Q3=238.1, collision energy=30.  
3  
4

5 **Computational modeling and crystallography** Available human cathepsin B structures in Protein  
6 Data Bank were analysed, and a structure bound covalently to a dipeptidyl nitrile inhibitor (PDB entry  
7 1GMY) was selected to guide the design of non-peptidic, cathepsin B-cleavable linkers. Specific  
8 interactions between the inhibitor and cathepsin B observed from the crystallographic structure inspired  
9 us to pursue two design strategies: 1) to replace the amide bond between the P1 and P2 moieties while  
10 maintaining the positions/interactions of their side chains; 2) to replace the P2 moiety while keeping the  
11 network of hydrogen bond interaction with residues Gly74 and Gly198 (Figure 1A and 1B). In both  
12 cases, a “Link Multiple Fragments” search was performed in MOE (Chemical Computing Group,  
13 v2012) using the default library to identify chemical structures that could connect the two fragments on  
14 either side of the moiety being replaced. Using MOE, the hits were filtered by pharmacophores defined  
15 by the observed interactions, energy-minimized in absence of the protein in order to identify highly-  
16 strained conformations, and then visually inspected in the enzyme active site. For a selected subset of  
17 candidate structures, the tetrahedral intermediate of linker hydrolysis with a p-amino benzyl alcohol  
18 leaving group were built in MOE based on the reported catalytic mechanism of cathepsin B (Figure 1C  
19 and 1D, Supporting Information Figure S1A and S1B).<sup>15,16</sup> The X-ray crystallographic structure of **28**  
20 (crystallized and determined by Proteros Biostructures, Germany) was refined at 1.6Å resolution to  
21  $R_{\text{free}}=17.6\%$  in space group P21. The data were twinned (twin fraction = 48.5%, twin operator: -H, -K,  
22 H+L). The coordinates were deposited under the accession code 6AY2 in Protein Data Bank.  
23  
24  
25  
26  
27  
28  
29  
30  
31  
32  
33  
34  
35  
36  
37  
38  
39  
40  
41  
42  
43  
44  
45  
46

47 **Synthesis of chemicals** Synthesis and characterization of compounds **1-36** are provided in  
48 Supporting Information. For all biologically evaluated compounds, the purity was determined by HPLC  
49 to be >95%.  
50  
51  
52  
53

54 **Conjugation process and characterization by mass spectrometry** Construction and production of  
55 the THIOMAB<sup>TM</sup> antibodies used were done as reported previously.<sup>24</sup> Briefly, an alanine-to-cysteine  
56  
57  
58  
59  
60

1 mutation was made at 118 (EU numbering) position of the heavy chain of the antibody to produce the  
2 corresponding THIOMAB™ antibody. The THIOMAB™ antibodies were conjugated to different linker  
3 drugs as described previously.<sup>24</sup> Briefly, the antibody was reduced in presence of fifty-fold molar  
4 excess DTT (Calbiochem) overnight. The reducing agent and the cysteine and glutathione blocks were  
5 purified away using HiTrap SP-HP column (GE Healthcare). The antibody was reoxidized in presence  
6 of fifteen-fold molar excess dhAA (MP Biomedical) for 2.5 hours. The formation of interchain disulfide  
7 bonds was monitored by LC/MS. Linker drug in range of threefold to tenfold molar excess over protein  
8 was incubated with the activated THIOMAB™ antibodies for 3 or 16 hours. The antibody drug  
9 conjugate was purified on HiTrap SP-HP column (GE Healthcare) to remove excess linker drug. The  
10 number of conjugated linker drug molecules per THIOMAB™ antibody was quantified by LC/MS  
11 analysis. Purity was also assessed by size exclusion chromatography. LC/MS analysis was performed  
12 on a 6530 Accurate-Mass Quadrupole Time-of-Flight (Q-TOF) LC/MS (Agilent Technologies).  
13 Samples were chromatographed on a PRLP-S, 1000 Å, 8 µm (50 mm 2.1 mm, Agilent Technologies)  
14 heated to 80 °C. A linear gradient from 30–60% B in 4.3 minutes (solvent A, 0.05% TFA in water;  
15 solvent B, 0.04% TFA in acetonitrile) was used and the eluent was directly ionized using the  
16 electrospray source. Data was collected and deconvoluted using the Agilent Mass Hunter qualitative  
17 analysis software. Before LC/MS analysis, antibody drug conjugate was treated with 15 mM DTT for  
18 30 minutes at pH 8.0, and 37 °C to separate the HC and LC portion for ease of analysis.  
19 Chromatographic conditions were chosen to achieve baseline resolution of LC, HC and HC+1 drug in  
20 different peaks. The drug to antibody ratio (DAR) was calculated using the integrated peak area of the  
21 UV chromatogram at 280 nm and orthogonally from the abundance of the ions present in LC/MS  
22 deconvoluted results. The peaks were identified using LC/MS. All ADCs in this study employed  
23 THIOMAB™ antibodies and the DAR values were determined to be between 1.8 and 2.0.

24  
25  
26  
27  
28  
29  
30  
31  
32  
33  
34  
35  
36  
37  
38  
39  
40  
41  
42  
43  
44  
45  
46  
47  
48  
49  
50  
51  
52  
53  
54 **Characterization of ADC activity in cell viability assay** Cells were plated in black-walled 96-well  
55 plates (4, 000 cells/100 µl for SK-BR-3 and MCF7 cells) and allowed to adhere overnight at 37°C in a  
56  
57  
58  
59  
60

1 humidified atmosphere of 5% CO<sub>2</sub>. Medium (Ham's F-12: high glucose DMEM [50:50] supplemented  
2 with 10% heat-inactivated fetal bovine serum and 2 mmol/L L-glutamine) (all from Invitrogen Corp.)  
3 was then removed and replaced by 100 µl fresh culture medium containing various concentrations of  
4 each conjugate (conjugate stock [in 20 mM histidine acetate pH 5.5, 240 mM sucrose, 0.02% Tween 20]  
5 diluted in medium). Cell Titer-Glo (Promega Corp.) was added to the wells at 5 days after drug  
6 administration and the luminescent signal was measured using EnVision Multilabel Plate Reader  
7 (PerkinElmer).  
8  
9  
10  
11  
12  
13  
14  
15

### 16 **Quantitation of ADC payload release in cell lines and the effect of protease inhibitor treatment**

17 Her2-expressing SKBR3 cells were seeded at were seeded at  $2.0 \times 10^5$  cells/mL in 50uL DMEM culture  
18 media supplemented with 10% fetal bovine serum and 2mM glutamine (Genentech Media Prep), in 96-  
19 well Costar plates and incubated at 37°C overnight in a CO<sub>2</sub> incubator. The next day, antibody drug  
20 conjugates (ADC) with Val-Cit or cBu-Cit linkers were diluted with the culture media at 2X final  
21 concentrations ranging from 0.16 µg/ml to 20 µg/ml were added to the plates, and incubated with cells  
22 for 2 or 23 hrs. After incubation, close to 100ul of media was removed from each well and transferred to  
23 a new deep-well plate, then mixed with 300 µl of 100% acetonitrile per sample. Immediately after the  
24 media removal, cell lysate samples were prepared with 200 µl of 75% acetonitrile to disrupt the cells  
25 and precipitate the protein. All lysed samples were centrifuged at 4,000 x g for 15min at 4°C. After  
26 centrifugation the 150uL supernant from cell lysate plate was transferred to a new plate, and 300uL  
27 from media plate supernatants into fresh 96-well plate, both plates were placed in the Turbo Vap  
28 concentration workstation to facilitate evaporation for and evaporated for 20 and 40min, respectively  
29 (N<sub>2</sub> gas flow rate 60 ft<sup>3</sup>/hr, heater temperature 50°C) using TurboVap® 96 (Biotage, Charlotte, NC).  
30 Pellets were reconstituted in 120uL of water (Optima™ LC/MS, Fisher Chemical), and centrifuged at  
31 4,000 x g for 15min at 4°C. The samples were then reconstituted with H<sub>2</sub>O. After centrifugation,  
32 100uL of each supernatant was transferred to a new 96-well plate. All samples were than analyzed using  
33 electrospray LC-MS/MS.  
34  
35  
36  
37  
38  
39  
40  
41  
42  
43  
44  
45  
46  
47  
48  
49  
50  
51  
52  
53  
54  
55  
56  
57  
58  
59  
60

1 LC-MS/MS analysis protocol: 10  $\mu$ L of the acidified samples were injected onto a Phenomenex Kinetex  
2 50 x 2.1 mm i.d. XB-C18 reversed phase column coupled to an Sciex 6500 QTRAP mass spectrometer  
3 system at a flow rate of 0.8 mL/min with the following gradient: 5% B (100% acetonitrile + 0.1%  
4 formic acid) at 0-0.5 min; 70% B at 1 min; 95% B at 1.1 min. The mass spectrometer Turbo Spray  
5 IonDrive Source temperature was 400  $^{\circ}$ C and the ion spray voltage 3500 V. The source parameters  
6 curtain gas, ion source gas 1 and ion source gas 2 were set at 35, 50 and 50 psi respectively. Multiple  
7 reaction monitoring (MRM) transitions  $m/z$  718.4  $\rightarrow$  134.2 (CE 43 V, CXP 8V), 718.4  $\rightarrow$  506.3 (CE 31  
8 V, CXP 14V), and 718.4  $\rightarrow$  686.3 (CE 39 V, CXP 18V) were used with dwell time 100 msec and  
9 declustering potential 46 V. And for internal control Loperamide MRM  $m/z$  477.15  $\rightarrow$  266.2 (CE 35 V,  
10 CXP 14V, declustering potential 116 V, dwell time 100 msec). Data was analyzed using MultiQuant  
11 software, and graphs were generated using Microsoft excel and GraphPad Prism 6.  
12  
13  
14  
15  
16  
17  
18  
19  
20  
21  
22  
23  
24  
25

26 For the protease inhibitor treatment experiment, SKBR3 cells were seeded at 80,000 cells/well onto the  
27 Costar plate as described above. ADC at 1  $\mu$ g/ml was added onto the plate in the presence of 50  $\mu$ M of  
28 inhibitor. All ADC-inhibitor combinations were incubated with cells overnight. Cell lysates were  
29 collected, prepared and then analyzed using electrospray LC-MS/MS as described above.  
30  
31  
32  
33  
34  
35

36 Inhibitors CA-074\_Me (catalog no. 205531), CAA0225 (catalog no. 2019502), and pepstatin (catalog  
37 no. 516481) were purchased from EMD Millipore Corp, (Billerica, MA). BML\_244 (catalog no.  
38 ab141723) was purchased from Abcam (Cambridge, MA), and leupeptin (catalog no. 78435) was from  
39 Fisher Scientific Co. (Pittsburgh, PA). The purities of the inhibitors were all above 95% by HPLC  
40 according to the vendors.  
41  
42  
43  
44  
45  
46  
47

48 **Efficacy study in mouse xenograft models** All animal studies were carried out in compliance with  
49 National Institutes of Health guidelines for the care and use of laboratory animals and were approved by  
50 the Institutional Animal Care and Use Committee at Genentech, Inc.  
51  
52  
53  
54  
55  
56  
57  
58  
59  
60

1 The efficacy of anti-CD22 drug conjugates was evaluated in a mouse xenograft model of CD22-  
2 expressing WSU-DLCL2 or Bjab-luc human non-Hodgkin lymphoma. The WSU-DLCL2 cell line was  
3  
4 obtained from DSMZ (German Collection of Microorganisms and Cell Cultures; Braunschweig,  
5  
6 Germany). The Bjab-luc cell line was obtained from Genentech cell line repository, and was  
7  
8 authenticated by short tandem repeat (STR) profiling using the Promega PowerPlex 16 System to  
9  
10 determine cell line ancestry.  
11  
12  
13

14  
15 To set up the WSU-DLCL2 or Bjab-luc xenograft model, tumor cells (20 million cells in 0.2mL  
16  
17 Hank's Balanced Salt Solution; Hyclone) were inoculated subcutaneously into the flanks of female C.B-  
18  
19 17 SCID mice (Charles Rivers Laboratories). The efficacy of anti-NaPi2b drug conjugates was  
20  
21 investigated in a mouse xenograft model of NaPi2b-expressing OVCAR3X2.1 human ovarian cancer.  
22  
23 The OVCAR3 cell line was obtained from ATCC (American Type Culture Collection; Manassas, VA)  
24  
25 and a sub-line OVCAR3X2.1 was generated at Genentech for optimal growth in mice. To set up the  
26  
27 OVCAR3X2.1 xenograft model, tumor cells (10 million cells in 0.2mL Hank's Balanced Salt Solution;  
28  
29 Hyclone) were inoculated in the thoracic mammary fat pad region of female C.B-17 SCID-beige mice  
30  
31 (Charles Rivers Laboratories). When the xenograft tumors reached the desired volume (day 0), animals  
32  
33 were divided into groups of 8 mice with similar mean tumor size and received a single intravenous  
34  
35 injection of antibody drug conjugates through the tail vein. The results were plotted as mean tumor  
36  
37 volume  $\pm$  SEM of each group over time. Blood samples were collected via retro-orbital bleeds and used  
38  
39 to derive plasma for PK analyses.  
40  
41  
42  
43  
44

45 **Sparse PK and in vivo ADC stability** Sparse pharmacokinetic sampling (collections at study days 1,  
46  
47 7 and 14 post-dose) was collected from efficacy study (12-3033A) to preliminarily assess exposure and  
48  
49 stability differences of these conjugates. The total antibody (TAB) is a measurement of the antibody,  
50  
51 and irrespective of the drug load, while the conjugated antibody (Conj. Ab) is measurement of the  
52  
53 antibody and stability of the linker. Both analytes were measured by ELISA as described previously.<sup>33</sup>  
54  
55 Total Antibody ELISA. Nunc® MaxiSorp™ 384-well plates (Nalge Nunc International, Rochester, NY)  
56  
57  
58  
59  
60

1 were coated with 0.33  $\mu\text{g/mL}$  6D3 anti-Idiotypic antibody (Genentech, South San Francisco, CA)  
2 diluted in coat buffer (0.05 M carbonate/bicarbonate buffer pH 9.6) and incubated overnight at 4oC. The  
3 plates were washed 3 times with wash buffer (0.5% Tween-20 in PBS buffer, pH 7.4) and treated with  
4 block buffer (PBS/0.5% BSA/15 ppm Proclin, pH 7.4) for 1 to 2 hours. The plates were again washed 3  
5 times with wash buffer and then samples diluted in sample diluent (PBS/0.5% BSA/0.05% Tween  
6 20/5mM EDTA/0.25% CHAPS/ 0.35M NaCl/15 ppm Proclin, pH 7.4) were added to the wells and  
7 incubated overnight at 4oC. The next day, the plates were brought to room temperature and then washed  
8 6 times with wash buffer. A detection antibody, sheep anti-human IgG conjugated to horseradish  
9 peroxidase (Jackson ImmunoResearch Laboratories, Inc., West Grove, PA), diluted to 120 ng/mL in  
10 assay buffer (PBS/0.5% BSA/15 ppm Proclin/0.05% Tween 20, pH7.4) was added to the wells and  
11 incubated on a shaker for 1 hour at 4oC. The plates were washed 6 times with wash buffer and  
12 developed using TMB peroxidase substrate (Moss Inc., Pasadena, Maryland) for 15 minutes followed  
13 by 1M Phosphoric acid to stop the reaction. Absorbance was measured at 450 nm against a reference  
14 wavelength of 620 nm. The assay range was 0.164 – 40 ng/mL with a minimum dilution of 1:100.  
15 (LOD = 16.4ng/mL)

16  
17  
18  
19  
20  
21  
22  
23  
24  
25  
26  
27  
28  
29  
30  
31  
32  
33  
34  
35  
36 **Supporting Information Available:** Three-dimensional coordinates of the models of the tetrahedral  
37 intermediate of hydrolysis for compounds **7**, **9** and **15**, as well as the chain A of PDB entry 1GMY are  
38 included as PDB-formatted files. Models for **7** and **9** are also shown in Figures S1A and S1B. Figure  
39 S2 shows the body weight data for the efficacy study in the CD22-expressing lymphoma model WSU-  
40 DLCL2. Table S1 reports the crystallographic data statistics. Synthesis and characterization of  
41 compounds **1-36** as well as a csv file of their SMILE strings are included.

42  
43  
44  
45  
46  
47  
48  
49  
50 **Accession Codes:** The X-ray crystallographic structure of **28** bound to human cathepsin B was  
51 deposited in the PDB under the accession code 6AY2. Authors will release the atomic coordinates and  
52 experimental data upon article publication.  
53  
54  
55  
56  
57  
58  
59  
60

**Corresponding Author Information:** Tel: (650) 467-8283; fax: (650) 225-2061; email: Wei.BinQing@gene.com

**Acknowledgement:** We thank Jack Sadowsky, Martine Darwish for helping in the preparation and analysis of some materials used in the study, Susan Spencer and Genee Lee for the coordinating the studies, and Peter S. Dragovich and Daniel F. Ortwine for reviewing the manuscript. Special thanks to James Kiefer for twin refinement of the cathepsin B structure in complex with **28**.

**Abbreviations:** ADC, antibody-drug-conjugate; Val-Cit, valine-citrulline; Val-Ala, valine-alanine; cBu, cyclobutane-1,1-dicarboxamide; MMAE, monomethyl auristatin; PBD, pyrrolobenzodiazepine dimer.

## References:

- (1) Junutula, J. R.; Gerber, H.-P. Next-Generation Antibody-Drug Conjugates (ADCs) for Cancer Therapy. *ACS Med. Chem. Lett.* **2016**, *7* (11), 972–973.
- (2) Saber, H.; Leighton, J. K. An FDA Oncology Analysis of Antibody-Drug Conjugates. *Regul. Toxicol. Pharmacol.* **2015**, *71* (3), 444–452.
- (3) Donaghy, H. Effects of Antibody, Drug and Linker on the Preclinical and Clinical Toxicities of Antibody-Drug Conjugates. *MAbs* **2016**, *8* (4), 659–671.
- (4) Shen, B.-Q.; Xu, K.; Liu, L.; Raab, H.; Bhakta, S.; Kenrick, M.; Parsons-Reponte, K. L.; Tien, J.; Yu, S.-F.; Mai, E.; Li, D.; Tibbitts, J.; Baudys, J.; Saad, O. M.; Scales, S. J.; McDonald, P. J.; Hass, P. E.; Eigenbrot, C.; Nguyen, T.; Solis, W. a; Fuji, R. N.; Flagella, K. M.; Patel, D.; Spencer, S. D.; Khawli, L. a; Ebens, A.; Wong, W. L.; Vandlen, R.; Kaur, S.; Sliwkowski, M. X.; Scheller, R. H.; Polakis, P.; Junutula, J. R. Conjugation Site Modulates the in Vivo Stability and Therapeutic Activity of Antibody-Drug Conjugates. *Nat. Biotechnol.* **2012**, *30* (2), 184–189.
- (5) Dorywalska, M.; Strop, P.; Melton-Witt, J. a.; Hasa-Moreno, A.; Farias, S. E.; Galindo Casas, M.; Delaria, K.; Lui, V.; Poulsen, K.; Loo, C.; Krimm, S.; Bolton, G.; Moine, L.; Dushin, R.; Tran, T.-T.; Liu, S.-H.; Rickert, M.; Foletti, D.; Shelton, D. L.; Pons, J.; Rajpal, A. Effect of Attachment Site on Stability of Cleavable Antibody Drug Conjugates. *Bioconjug. Chem.* **2015**, 150220133437002.
- (6) Cohen, R.; Vugts, D. J.; Visser, G. W. M.; Stigter-van Walsum, M.; Bolijn, M.; Spiga, M.; Lazzari, P.; Shankar, S.; Sani, M.; Zanda, M.; van Dongen, G. A. M. S. Development of Novel ADCs: Conjugation of Tubulysin Analogues to Trastuzumab Monitored by Dual Radiolabeling. *Cancer Res.* **2014**, *74* (20), 5700–5710.
- (7) Beck, A.; Wurch, T.; Bailly, C.; Corvaia, N. Strategies and Challenges for the next Generation of Therapeutic Antibodies. *Nat. Rev. Immunol.* **2010**, *10* (5), 345–352.

- 1  
2  
3  
4  
5  
6  
7  
8  
9  
10  
11  
12  
13  
14  
15  
16  
17  
18  
19  
20  
21  
22  
23  
24  
25  
26  
27  
28  
29  
30  
31  
32  
33  
34  
35  
36  
37  
38  
39  
40  
41  
42  
43  
44  
45  
46  
47  
48  
49  
50  
51  
52  
53  
54  
55  
56  
57  
58  
59  
60
- (8) Dubowchik, G. M.; Firestone, R. A.; Padilla, L.; Willner, D.; Hofstead, S. J.; Mosure, K.; Knipe, J. O.; Lasch, S. J.; Trail, P. A. Cathepsin B-Labile Dipeptide Linkers for Lysosomal Release of Doxorubicin from Internalizing Immunoconjugates: Model Studies of Enzymatic Drug Release and Antigen-Specific in Vitro Anticancer Activity. *Bioconjug. Chem.* **2002**, *13* (4), 855–869.
  - (9) Senter, P. D.; Sievers, E. L. The Discovery and Development of Brentuximab Vedotin for Use in Relapsed Hodgkin Lymphoma and Systemic Anaplastic Large Cell Lymphoma. *Nat. Biotechnol.* **2012**, *30* (7), 631–637.
  - (10) Jain, N.; Smith, S. W.; Ghone, S.; Tomczuk, B. Current ADC Linker Chemistry. *Pharmaceutical Research.* **2015**, 3526–3540.
  - (11) Dal Corso, A.; Cazzamalli, S.; Gébleux, R.; Mattarella, M.; Neri, D. Protease-Cleavable Linkers Modulate the Anticancer Activity of Noninternalizing Antibody-Drug Conjugates. *Bioconjug. Chem.* **2017**, *28* (7), 1826–1833.
  - (12) Singh, R.; Setiady, Y. Y.; Ponte, J.; Kovtun, Y. V.; Lai, K. C.; Hong, E. E.; Fishkin, N.; Dong, L.; Jones, G. E.; Coccia, J. A.; Lanieri, L.; Veale, K.; Costoplus, J. A.; Skaletskaya, A.; Gabriel, R.; Salomon, P.; Wu, R.; Qiu, Q.; Erickson, H. K.; Lambert, J. M.; Chari, R. V.; Widdison, W. C. A New Triglycyl Peptide Linker for Antibody-Drug Conjugates (ADCs) with Improved Targeted Killing of Cancer Cells. *Mol Cancer Ther* **2016**, *15* (6), 1311–1320.
  - (13) Puthenveetil, S.; He, H.; Loganzo, F.; Musto, S.; Teske, J.; Green, M.; Tan, X.; Hosselet, C.; Lucas, J.; Tumey, L. N.; Sapra, P.; Subramanyam, C.; O'Donnell, C. J.; Graziani, E. I. Multivalent Peptidic Linker Enables Identification of Preferred Sites of Conjugation for a Potent Thialanstatin Antibody Drug Conjugate. *PLoS One* **2017**, *12* (5), 1–16.
  - (14) Rawlings, N. D.; Barrett, A. J.; Finn, R. Twenty Years of the MEROPS Database of Proteolytic Enzymes, Their Substrates and Inhibitors. *Nucleic Acids Res.* **2016**, *44* (D1), D343–D350.
  - (15) Musil, D.; Zucic, D.; Turk, D.; Engh, R. a; Mayr, I.; Huber, R.; Popovic, T.; Turk, V.; Towatari, T.; Katunuma, N. The Refined 2.15 Å X-Ray Crystal Structure of Human Liver Cathepsin B: The Structural Basis for Its Specificity. *EMBO J.* **1991**, *10* (9), 2321–2330.
  - (16) Illy, C.; Quraishi, O.; Wang, J.; Purisima, E.; Vernet, T.; Mort, J. S. Role of the Occluding Loop in Cathepsin B Activity. *J. Biol. Chem.* **1997**, *272* (2), 1197–1202.
  - (17) Mohamed, M. M.; Sloane, B. F. Cysteine Cathepsins: Multifunctional Enzymes in Cancer. *Nat. Rev. Cancer* **2006**, *6* (10), 764–775.
  - (18) Gondi, C. S.; Rao, J. S. Cathepsin B as a Cancer Target. *Expert Opin. Ther. Targets* **2013**, *17* (3), 281–291.
  - (19) Roshy, S.; Sloane, B. F.; Moin, K. Pericellular Cathepsin B and Malignant Progression. *Cancer and Metastasis Reviews.* **2003**, 271–286.
  - (20) Mitrović, A.; Mirković, B.; Sosič, I.; Gobec, S.; Kos, J. Inhibition of Endopeptidase and Exopeptidase Activity of Cathepsin B Impairs Extracellular Matrix Degradation and Tumour Invasion. *Biol. Chem.* **2016**, *397* (2), 164–174.
  - (21) Cezari, M. H. S.; Puzer, L.; Juliano, M. A.; Carmona, A. K.; Juliano, L. Cathepsin B Carboxydipeptidase Specificity Analysis Using Internally Quenched Fluorescent Peptides. *Biochem. J.* **2002**, *368* (Pt 1), 365–369.
  - (22) Choe, Y.; Leonetti, F.; Greenbaum, D. C.; Lecaille, F.; Bogyo, M.; Brömme, D.; Ellman, J. A.;

Craik, C. S. Substrate Profiling of Cysteine Proteases Using a Combinatorial Peptide Library Identifies Functionally Unique Specificities. *J. Biol. Chem.* **2006**, *281* (18), 12824–12832.

- (23) Greenspan, P. D.; Clark, K. L.; Tommasi, R. A.; Cowen, S. D.; McQuire, L. W.; Farley, D. L.; Van Duzer, J. H.; Goldberg, R. L.; Zhou, H.; Du, Z.; Fitt, J. J.; Coppa, D. E.; Fang, Z.; Macchia, W.; Zhu, L.; Capparelli, M. P.; Goldstein, R.; Wigg, A. M.; Doughty, J. R.; Bohacek, R. S.; Knap, A. K. Identification of Dipeptidyl Nitriles as Potent and Selective Inhibitors of Cathepsin B through Structure-Based Drug Design. *J. Med. Chem.* **2001**, *44* (26), 4524–4534.
- (24) Junutula, J. R.; Raab, H.; Clark, S.; Bhakta, S.; Leipold, D. D. D.; Weir, S.; Chen, Y.; Simpson, M.; Tsai, S. P.; Dennis, M. S.; Lu, Y.; Meng, Y. G.; Ng, C.; Yang, J.; Lee, C. C.; Duenas, E.; Gorrell, J.; Katta, V.; Kim, A.; McDorman, K.; Flagella, K.; Venook, R.; Ross, S.; Spencer, S. D.; Lee Wong, W.; Lowman, H. B.; Vandlen, R.; Sliwkowski, M. X.; Scheller, R. H.; Polakis, P.; Mallet, W. Site-Specific Conjugation of a Cytotoxic Drug to an Antibody Improves the Therapeutic Index. *Nat. Biotechnol.* **2008**, *26* (8), 925–932.
- (25) Vollmar, B. S.; Wei, B.; Ohri, R.; Zhou, J.; He, J.; Yu, S.-F.; Leipold, D.; Cosino, E.; Yee, S.; Fourie-O'Donohue, A.; Li, G.; Lewis Phillips, G. D.; Kozak, K. R.; Kamath, A.; Xu, K.; Lee, G.; Lazar, G. A.; Erickson, H. K. Attachment Site Cysteine Thiol pKa Is a Key Driver for Site-Dependent Stability of THIOMAB™ Antibody-Drug Conjugates. *Bioconjug. Chem.* **2017**, *28* (10), 2538–2548.
- (26) Doronina, S. O.; Toki, B. E.; Torgov, M. Y.; Mendelsohn, B. a; Cerveny, C. G.; Chace, D. F.; DeBlanc, R. L.; Gearing, R. P.; Bovee, T. D.; Siegall, C. B.; Francisco, J. a; Wahl, A. F.; Meyer, D. L.; Senter, P. D. Development of Potent Monoclonal Antibody Auristatin Conjugates for Cancer Therapy. *Nat. Biotech.* **2003**, *21* (7), 778–784.
- (27) Montaser, M.; Lalmanach, G.; Mach, L. CA-074, but Not Its Methyl Ester CA-074Me, Is a Selective Inhibitor of Cathepsin B within Living Cells. *Biol. Chem.* **2002**, *383* (7–8), 1305–1308.
- (28) Takahashi, K.; Ueno, T.; Tanida, I.; Minematsu-Ikeguchi, N.; Murata, M.; Kominami, E. Characterization of CAA0225, a Novel Inhibitor Specific for Cathepsin L, as a Probe for Autophagic Proteolysis. *Biol. Pharm. Bull.* **2009**, *32* (3), 475–479.
- (29) Desmarais, S.; Massé, F.; Percival, M. D. Pharmacological Inhibitors to Identify Roles of Cathepsin K in Cell-Based Studies: A Comparison of Available Tools. *Biol. Chem.* **2009**, *390* (9), 941–948.
- (30) Marcinišzyn, J.; Hartsuck, J. A.; Tang, J. Mode of Inhibition of Acid Proteases by Pepstatin. *J. Biol. Chem.* **1976**, *251* (22), 7088–7094.
- (31) Libby, P.; Goldberg, a L. Leupeptin, a Protease Inhibitor, Decreases Protein Degradation in Normal and Diseased Muscles. *Science* (80-. ). **1978**, *199* (4328), 534–536.
- (32) Gregson, S. J.; Howard, P. W.; Hartley, J. A.; Brooks, N. A.; Adams, L. J.; Jenkins, T. C.; Kelland, L. R.; Thurston, D. E. Design, Synthesis, and Evaluation of a Novel Pyrrolobenzodiazepine DNA-Interactive Agent with Highly Efficient Cross-Linking Ability and Potent Cytotoxicity. *J. Med. Chem.* **2001**, *44* (5), 737–748.
- (33) Kaur, S.; Xu, K.; Saad, O. M.; Dere, R. C.; Carrasco-Triguero, M. Bioanalytical Assay Strategies for the Development of Antibody–drug Conjugate Biotherapeutics. *Bioanalysis* **2013**, *5* (2), 201–226.

1  
2  
3  
4  
5  
6  
7  
8  
9  
10  
11  
12  
13  
14  
15  
16  
17  
18  
19  
20  
21  
22  
23  
24  
25  
26  
27  
28  
29  
30  
31  
32  
33  
34  
35  
36  
37  
38  
39  
40  
41  
42  
43  
44  
45  
46  
47  
48  
49  
50  
51  
52  
53  
54  
55  
56  
57  
58  
59  
60

**Scheme 1. A simplified molecular construct for measuring the cleavage of ADC linker moieties by protease.** Reduction of ADC to the simplified construct is illustrated using the dipeptide linker Val-Cit (compound 1).

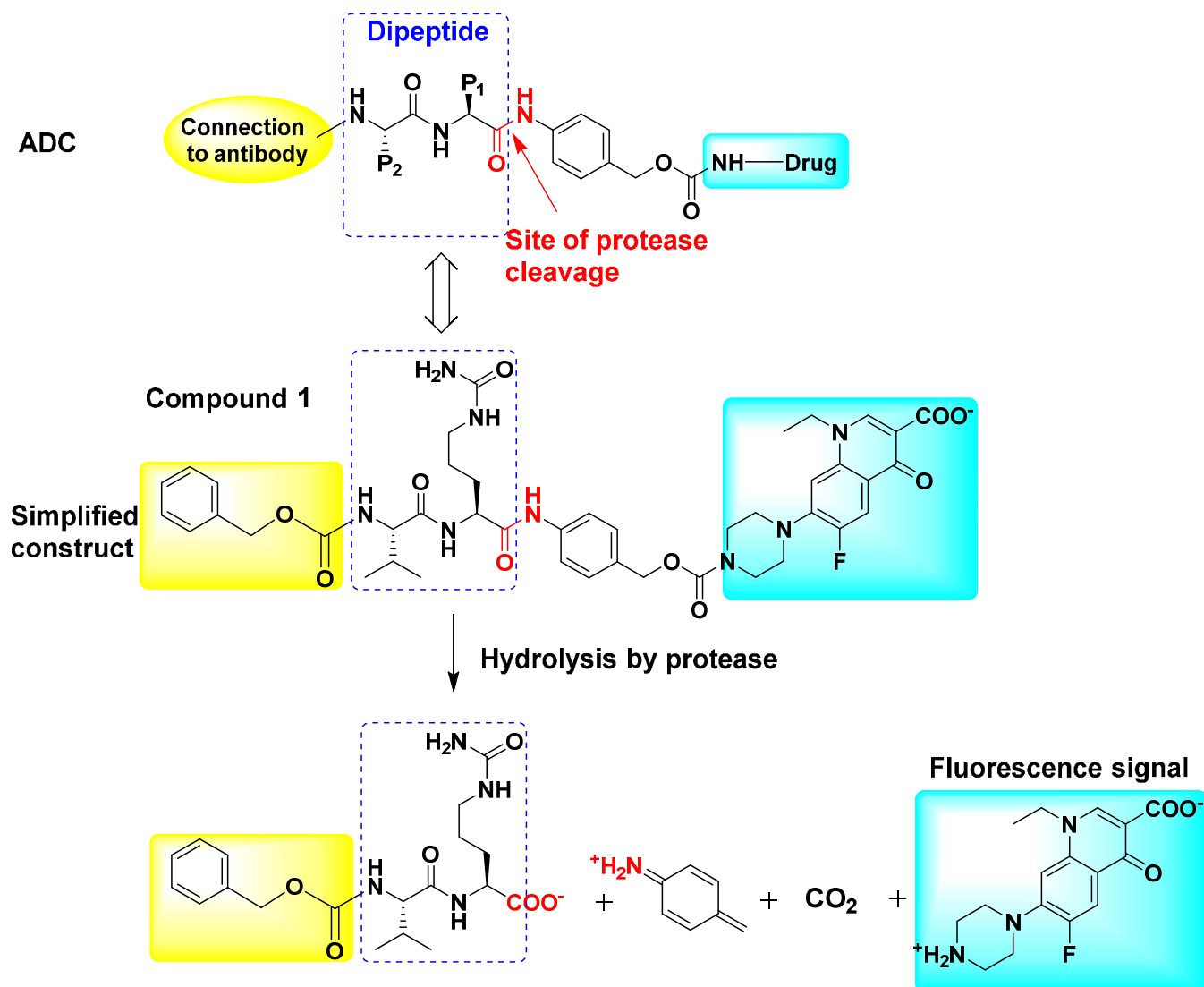
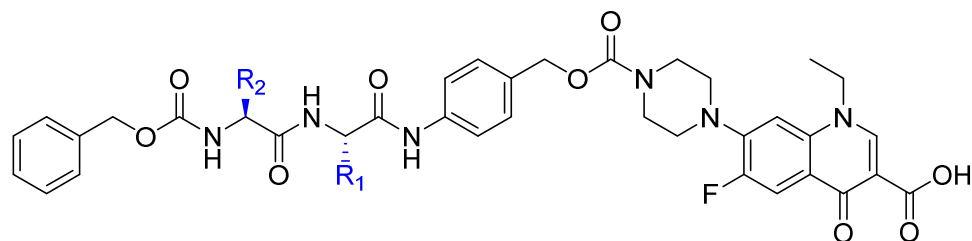


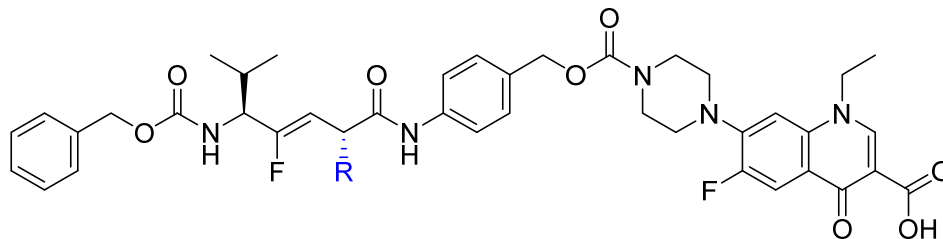
**Table 1.  $V_{\max}$  and  $K_m$  properties for the cleavage of representative dipeptide linkers by cathepsin B measured using the simplified constructs.**



| Ex | R <sub>1</sub> | R <sub>2</sub> | Cathepsin B cleavage <sup>a</sup> |                       |                |
|----|----------------|----------------|-----------------------------------|-----------------------|----------------|
|    |                |                | $V_{\max}^b$<br>(pmol/min)        | $K_m^b$<br>( $\mu$ M) | $V_{\max}/K_m$ |
| 1  |                |                | 2.7 (2.1, 3.2)                    | 64 (41, 87)           | 0.042          |
| 2  |                |                | 0.33 (0.27, 0.39)                 | 23 (12, 34)           | 0.014          |
| 3  |                |                | 2.1 (1.7, 2.6)                    | 5.7 (0.92, 10)        | 0.38           |
| 4  |                |                | 1.3 (1.2, 1.4)                    | 52 (44, 59)           | 0.025          |
| 5  |                |                | 0.054 (0.050, 0.058)              | 2.5 (1.7, 3.3)        | 0.021          |
| 6  |                |                | 0.16 (0.15, 0.17)                 | 5.0 (3.3, 6.7)        | 0.032          |

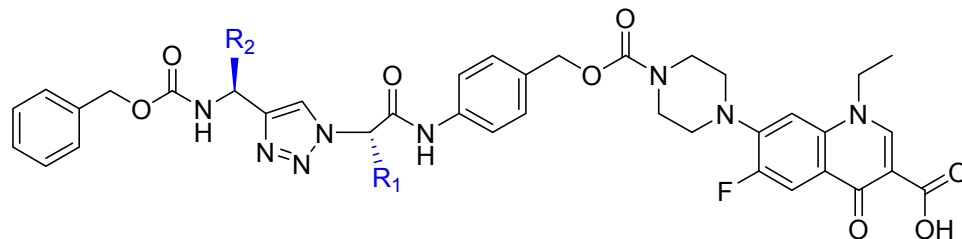
<sup>a</sup>The concentration of human cathepsin B enzyme was kept constant at 2nM. <sup>b</sup> $V_{\max}$  and  $K_m$  values were obtained by fitting the cleavage assay data (duplicate, n=1) using Michaelis-Menten equation. All values are rounded to two significant digits (95% confidence intervals given in parentheses).

**Table 2.  $V_{\max}$  and  $K_m$  properties for the cleavage of fluoro-olefin linkers by cathepsin B measured using the simplified constructs.**



| Ex | R    | Cathepsin B cleavage <sup>a</sup> |                       |                |
|----|------|-----------------------------------|-----------------------|----------------|
|    |      | $V_{\max}^b$<br>(pmol/min)        | $K_m^b$<br>( $\mu$ M) | $V_{\max}/K_m$ |
| 7  |      | 0.44 (0.28, 0.60)                 | 400 (180, 630)        | 0.0011         |
| 8  | •-Me | 1.2E-3 (8.0E-4, 1.6E-3)           | 6.4 (2.5, 10)         | 1.9E-4         |

<sup>a</sup>The concentration of human cathepsin B enzyme was kept constant at 2nM. <sup>b</sup> $V_{\max}$  and  $K_m$  values were obtained by fitting the cleavage assay data (duplicate, n=1) using Michaelis-Menten equation. All values are rounded to two significant digits (95% confidence intervals given in parentheses).

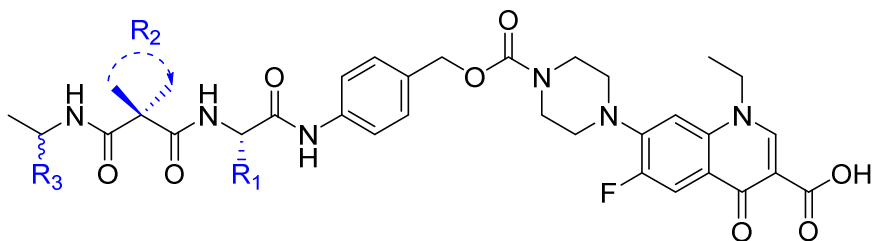
**Table 3.  $V_{\max}$  and  $K_m$  properties for the cleavage of triazole linkers by cathepsin B measured using the simplified constructs.**

| Ex | R <sub>1</sub> | R <sub>2</sub> | Cathepsin B cleavage <sup>a</sup> |                       |                 |
|----|----------------|----------------|-----------------------------------|-----------------------|-----------------|
|    |                |                | $V_{\max}^b$<br>(pmol/min)        | $K_m^b$<br>( $\mu$ M) | $V_{\max}/K_m$  |
| 9  |                |                | 1.3E-3 (8.1E-4, 1.9E-3)           | 6.7 (2.8, 11)         | 2.0E-4          |
| 10 |                |                | 0.020 (0.018, 0.022)              | 3.5 (2.1, 4.9)        | 5.7E-3          |
| 11 |                |                | 0.031 (0.026, 0.036)              | 8.8 (4.1, 13)         | 3.5E-3          |
| 12 |                |                | 3.4E-3 (1.4E-3, 5.3E-3)           | 31 (14, 48)           | 1.1E-4          |
| 13 |                |                | ND <sup>c</sup>                   | ND <sup>c</sup>       | ND <sup>c</sup> |

<sup>a</sup>The concentration of human cathepsin B enzyme was kept constant at 2nM. <sup>b</sup> $V_{\max}$  and  $K_m$  values were obtained by fitting the cleavage assay data (duplicate, n=1) using Michaelis-Menten equation. All values are rounded to two significant digits (95% confidence intervals given in parentheses). <sup>c</sup>Not determined because the cleavage activity was too low to be measured under the assay condition.

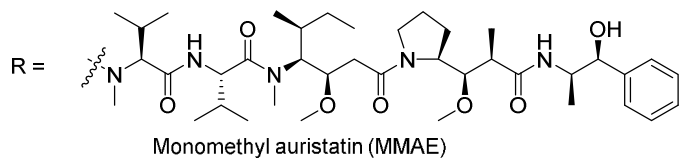
1  
2 **Table 4.  $V_{\max}$  and  $K_m$  properties for the cleavage of cycloalkyl-1,1-dicarboxamide linkers by**  
3 **cathepsin B measured using the simplified constructs.**  
4

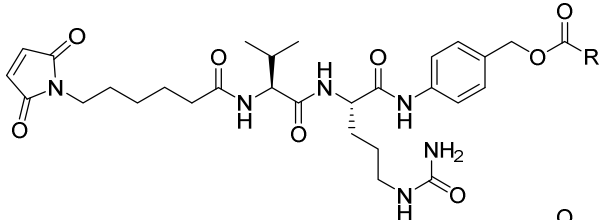
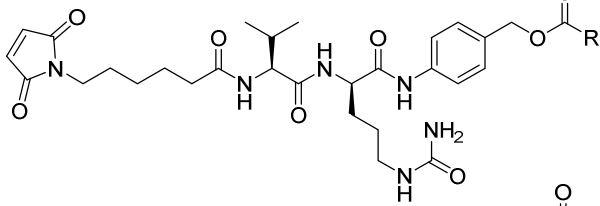
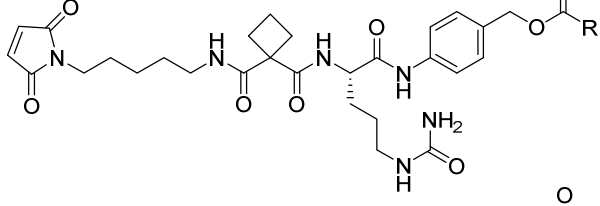
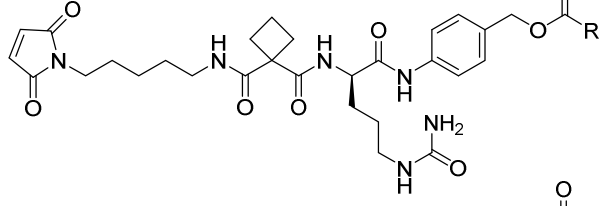
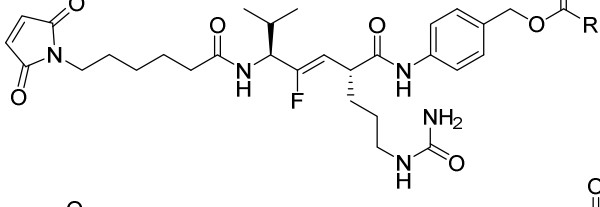
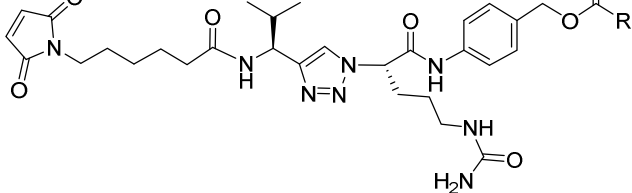
5 <sup>a</sup>The concentration of human cathepsin B enzyme was kept constant at 2nM. <sup>b</sup> $V_{\max}$  and  $K_m$  values were  
6 obtained by fitting the cleavage assay data (duplicate, n=1) using Michaelis-Menten equation. All  
7 values are rounded to two significant digits (95% confidence intervals given in parentheses). <sup>c</sup>Not  
8 determined because the cleavage activity was too low to be measured under the assay conditions. <sup>d</sup>**25**  
9 and **26** are a pair of diastereomers with unknown stereochemistry. <sup>e</sup>**28** is a single diastereomer with  
10 unknown stereochemistry at one of the chiral centers. It was used in the crystallography study as a  
11 mimic of the cBu-Cit linker.  
12  
13  
14  
15  
16  
17  
18  
19  
20  
21  
22  
23  
24  
25  
26  
27  
28  
29  
30  
31  
32  
33  
34  
35  
36  
37  
38  
39  
40  
41  
42  
43  
44  
45  
46  
47  
48  
49  
50  
51  
52  
53  
54  
55  
56  
57  
58  
59  
60



| Ex              | R <sub>1</sub> | R <sub>2</sub> | R <sub>3</sub> | Cathepsin B cleavage <sup>a</sup>           |                                     |                                  |
|-----------------|----------------|----------------|----------------|---|-------------------------------------|----------------------------------|
|                 |                |                |                | V <sub>max</sub> <sup>b</sup><br>(pmol/min) | K <sub>m</sub> <sup>b</sup><br>(μM) | V <sub>max</sub> /K <sub>m</sub> |
| 14              |                |                | H              | 0.022 (0.015, 0.029)                        | 86 (45, 130)                        | 2.6E-4                           |
| 15              |                |                | H              | 0.28 (0.20, 0.36)                           | 91 (48, 130)                        | 3.1E-3                           |
| 16              |                |                | H              | 0.12 (0.077, 0.16)                          | 67 (25, 110)                        | 1.8E-3                           |
| 17              |                |                | H              | 0.050 (0.030, 0.069)                        | 55 (14, 97)                         | 9.0E-4                           |
| 18              |                |                | H              | ND <sup>c</sup>                             | ND <sup>c</sup>                     | ND <sup>c</sup>                  |
| 19              |                |                | H              | 2.6 (1.9, 3.3)                              | 110 (62, 160)                       | 0.023                            |
| 20              |                |                | H              | 1.3 (0.55, 2.0)                             | 320 (130, 510)                      | 4.0E-3                           |
| 21              |                |                | H              | 2.7 (2.1, 3.2)                              | 280 (200, 350)                      | 9.7E-3                           |
| 22              |                |                | H              | 0.052 (0.043, 0.061)                        | 30 (18, 42)                         | 1.7E-3                           |
| 23              |                |                | H              | ND <sup>c</sup>                             | ND <sup>c</sup>                     | ND <sup>c</sup>                  |
| 24              |                |                |                | 0.14 (0.11, 0.16)                           | 45 (29, 62)                         | 3.1E-3                           |
| 25 <sup>d</sup> |                |                |                | 0.3 (0.27, 0.33)                            | 9.7 (6.2, 13)                       | 0.031                            |
| 26 <sup>d</sup> |                |                |                | 0.045 (0.040, 0.050)                        | 11 (6.8, 15)                        | 4.2E-3                           |
| 27              |                |                |                | 0.23 (0.19, 0.26)                           | 16 (9.8, 23)                        | 0.014                            |
| 28 <sup>e</sup> |                |                |                | NA  | NA                                  | NA                               |

**Table 5. Structures of the linker-MMAE molecules used to prepare the ADCs tested in biological studies.** All ADCs were conjugated via the maleimide group to an engineered cysteine at position 118 (EU numbering) on the two heavy chains of the respective antibodies.



| Ex | Alias            | Structure  |
|----|------------------|--|
| 29 | Val-Cit MMAE     |     |
| 30 | Val-(R)-Cit MMAE |     |
| 31 | cBu-Cit MMAE     |    |
| 32 | cBu-(R)-Cit MMAE |   |
| 33 | F-olefin MMAE    |   |
| 34 | Triazole MMAE    |  |



1 **Figure 1. Structure-based design of cathepsin B-cleavable, nonpeptidic ADC linkers.** A and B, PDB  
2 entry 1GMY shows that a network of hydrogen bonds are involved in proper positioning of a substrate  
3 for nucleophilic attack by the thiol of Cys29 residue. Modeling based on the structure led to three series  
4 of new linkers: the F-olefin, the triazole, and the cBu series. The inhibitor (carbon atoms colored in  
5 green) forms a thioimidate adduct with the protein, mimicking the acyl enzyme intermediate of substrate  
6 hydrolysis. Orange dotted lines show selected hydrogen bonds mentioned in the text. The moieties  
7 corresponding to the P1 and P2 side chains of a peptide substrate are labeled in blue in the chemical  
8 sketch. The scissile amide bond is in red. C and D, A model of the tetrahedral intermediate of  
9 hydrolysis for a cBu linker with a p-amino benzyl alcohol leaving group (**15**, carbon atoms in cyan).  
10 Orange dotted lines show selected hydrogen bonds mentioned in the text. The 1,1-dicarboxamide  
11 moiety is predicted to form the same hydrogen bonds with the protein as the PDB compound while the  
12 cyclobutyl group is expected to occupy the S2 site. The norfloxacin moiety is too far from the active  
13 site to participate in the amide bond hydrolysis, so it is omitted in the figure for clarity. E and F, X-ray  
14 crystal structure of human cathepsin B in complex with **28**, a covalent inhibitor analogous to the cBu-  
15 Cit linker, refined at 1.6Å resolution. The Polder omit electron density map contoured at 2.8σ is shown  
16 as blue mesh. Orange dotted lines show select hydrogen bonds mentioned in the text.  
17  
18  
19  
20  
21  
22  
23  
24  
25  
26  
27  
28  
29  
30  
31  
32  
33  
34  
35  
36  
37  
38  
39  
40  
41  
42  
43  
44  
45  
46  
47  
48  
49  
50  
51  
52  
53  
54  
55  
56  
57  
58  
59  
60

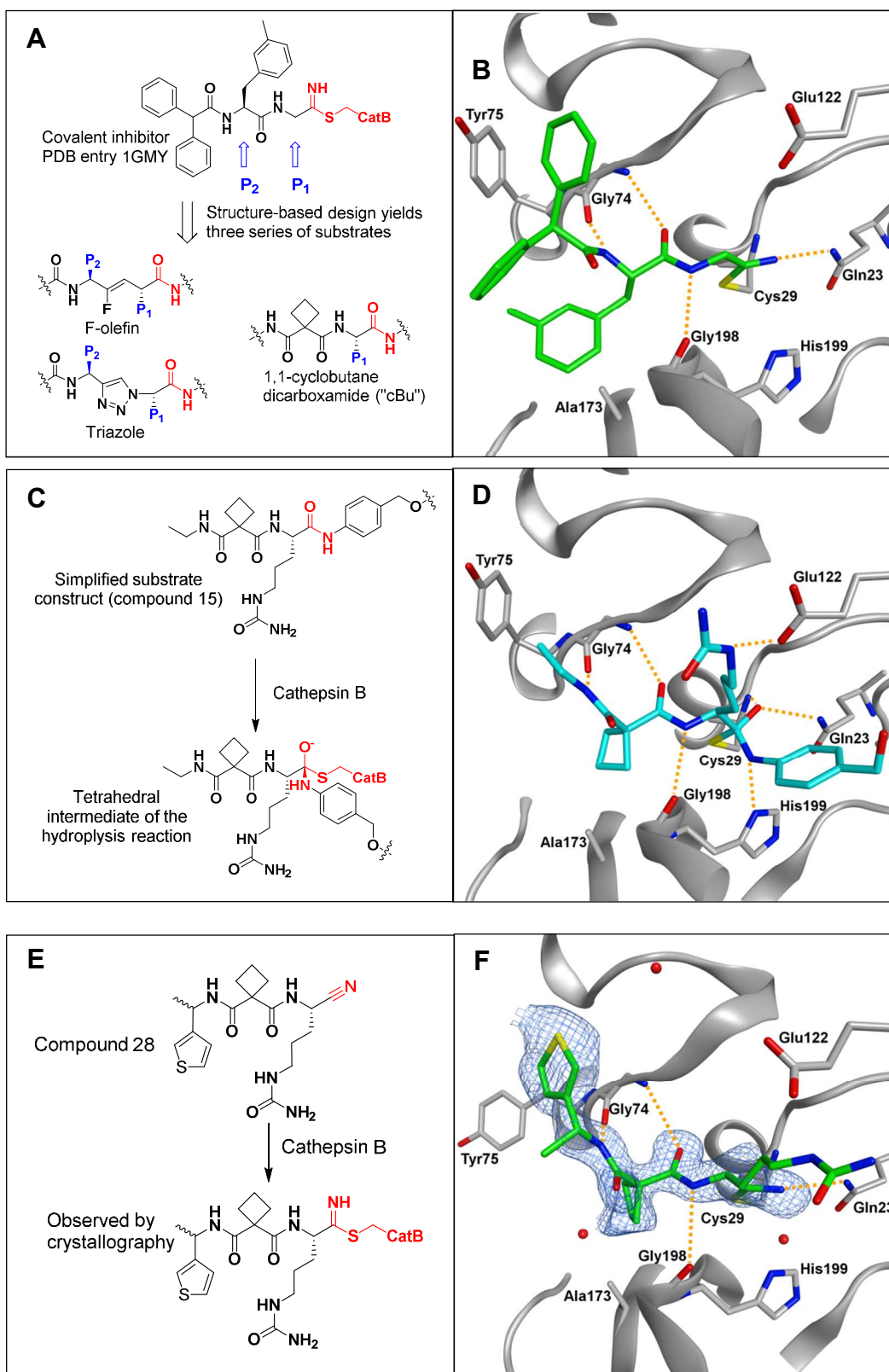


**Figure 2. Comparison of  $V_{\max}$  and  $K_m$  properties across all series.** Data from Tables 1 to 4 are plotted. Chemical series are color-coded: peptides from Table 1 are in red, fluoroolefins from Table 2 in magenta, 1,2,3-triazoles from Table 3 in orange, and cycloalkyl-1,1-dicarboxamides from Table 4 in green. For reference, compounds Val-Cit (**1**), Val-Ala (**2**), Val-Arg (**3**), cBu-Cit (**15**) and cBu-Arg (**19**) are labeled, and three different levels of  $V_{\max}/K_m$  ratio are shown by black lines. Compounds on the same line share the same  $V_{\max}/K_m$  value.

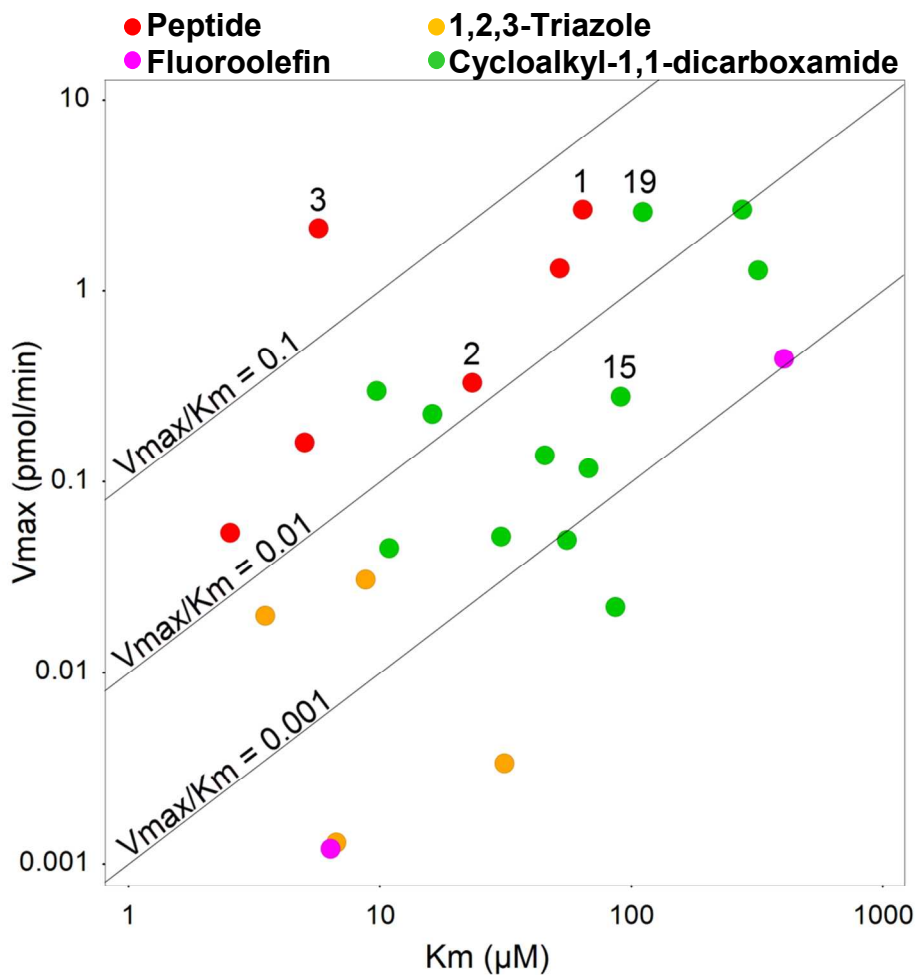


**Figure 3. Comparison of ADCs bearing different linkers in their anti-proliferation potencies and intracellular concentrations of the released payload in SK-BR-3 cancer cell line.** MMAE drug was conjugated to anti-Her2 and anti-CD22 (control) monoclonal antibodies via the Val-Cit and cBu-Cit linker, respectively (mAb-29, mAb-31). A, Cell viability after 5 days of ADC treatment. Each sample was in quadruplicate. B, The intracellular concentrations of the released MMAE in SK-BR-3 cells measured at 23 hours after the treatment with the ADCs. For comparison, ADCs bearing Val-(R)-Cit or cBu-(R)-Cit linker were also included (mAb-30, mAb-32). Each sample was in triplicate.

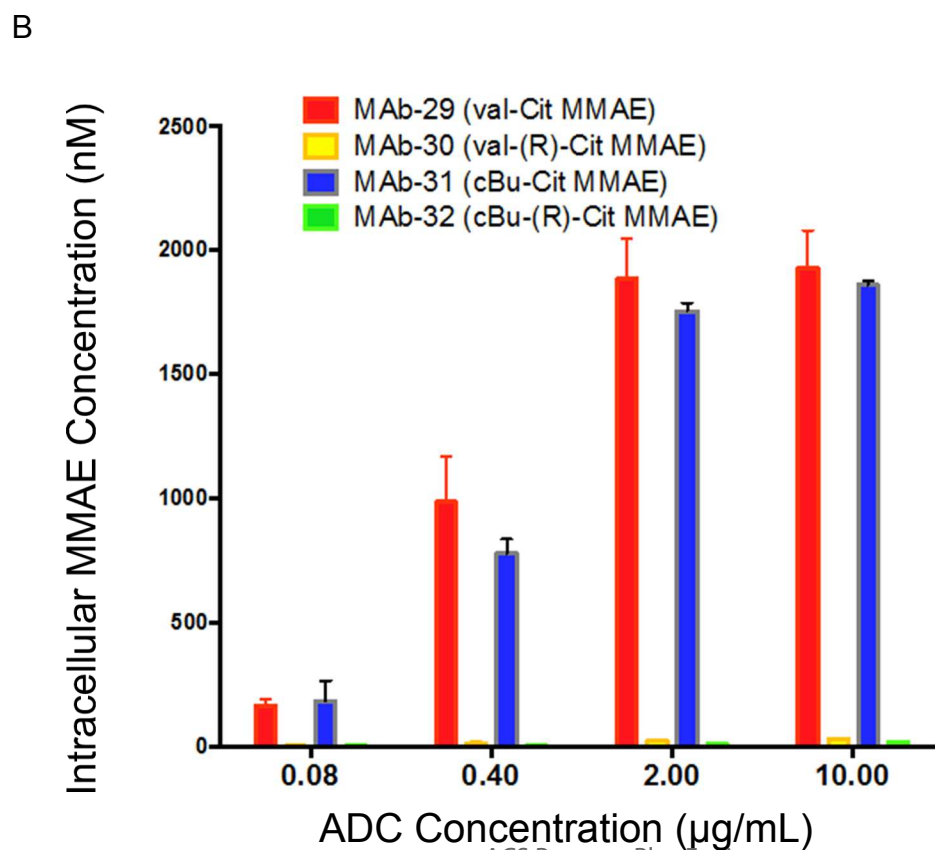
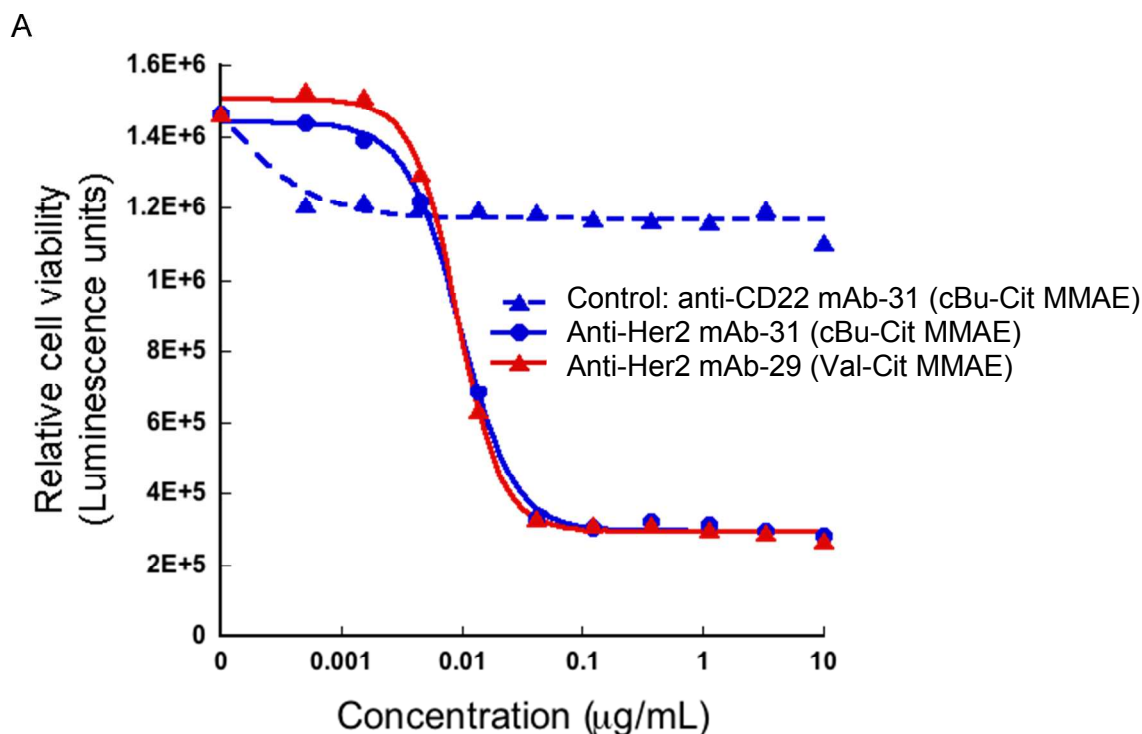


**Figure 4. Effect of protease inhibitors on the release of MMAE payload by ADCs bearing different linkers.** SK-BR-3 cells were treated overnight with 1 $\mu$ g/mL of anti-Her2 ADC carrying one of the four linker-MMAEs (**29**, **31**, **33**, or **34**) and 50 $\mu$ M of a protease inhibitor. Cell lysates were then prepared and analyzed by LC-MS/MS. Intracellular MMAE levels were quantified by total ion chromatogram (TIC), and for each linker-MMAE, all inhibitor-treated samples were normalized to the respective DMSO-treated control (100% TIC). Each sample was in triplicate except for the DMSO treated controls (n=4, in black).

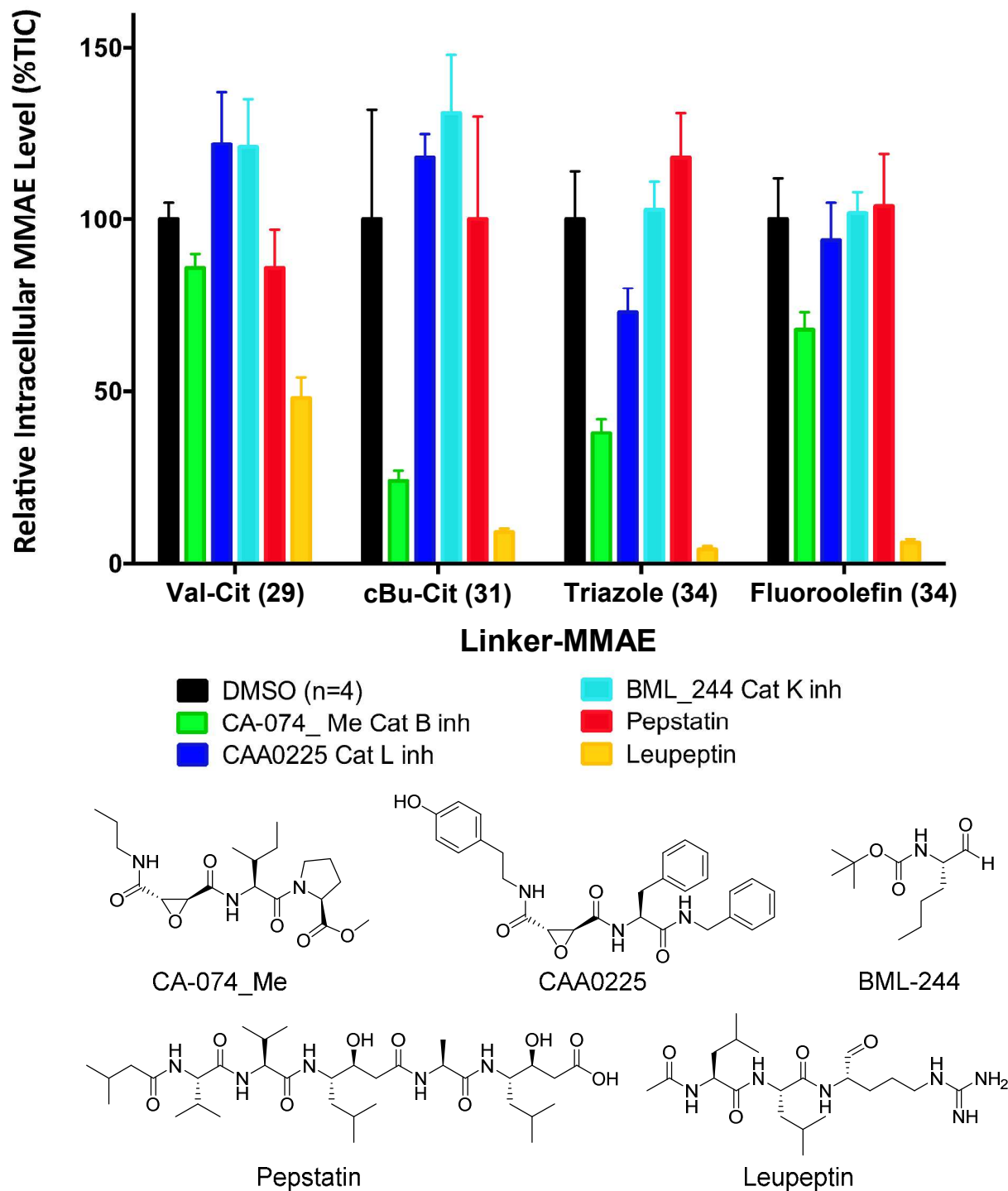


**Figure 5. Comparison of ADC efficacies in mouse xenograft tumor models.** A. In vivo efficacy of the anti-CD22 ADCs carrying MMAE payload were assessed in mice bearing WSU-DLCL2 (A) or Bjab-luc (B) human lymphoma xenografts. C. In vivo efficacy of the anti-Napi2b ADCs carrying PBD dimer payload were evaluated in mice bearing OVCAR3X2.1 human ovarian xenografts. In each study, animals received on day 0 a single intravenous injection of antibody drug conjugates through the tail vein.

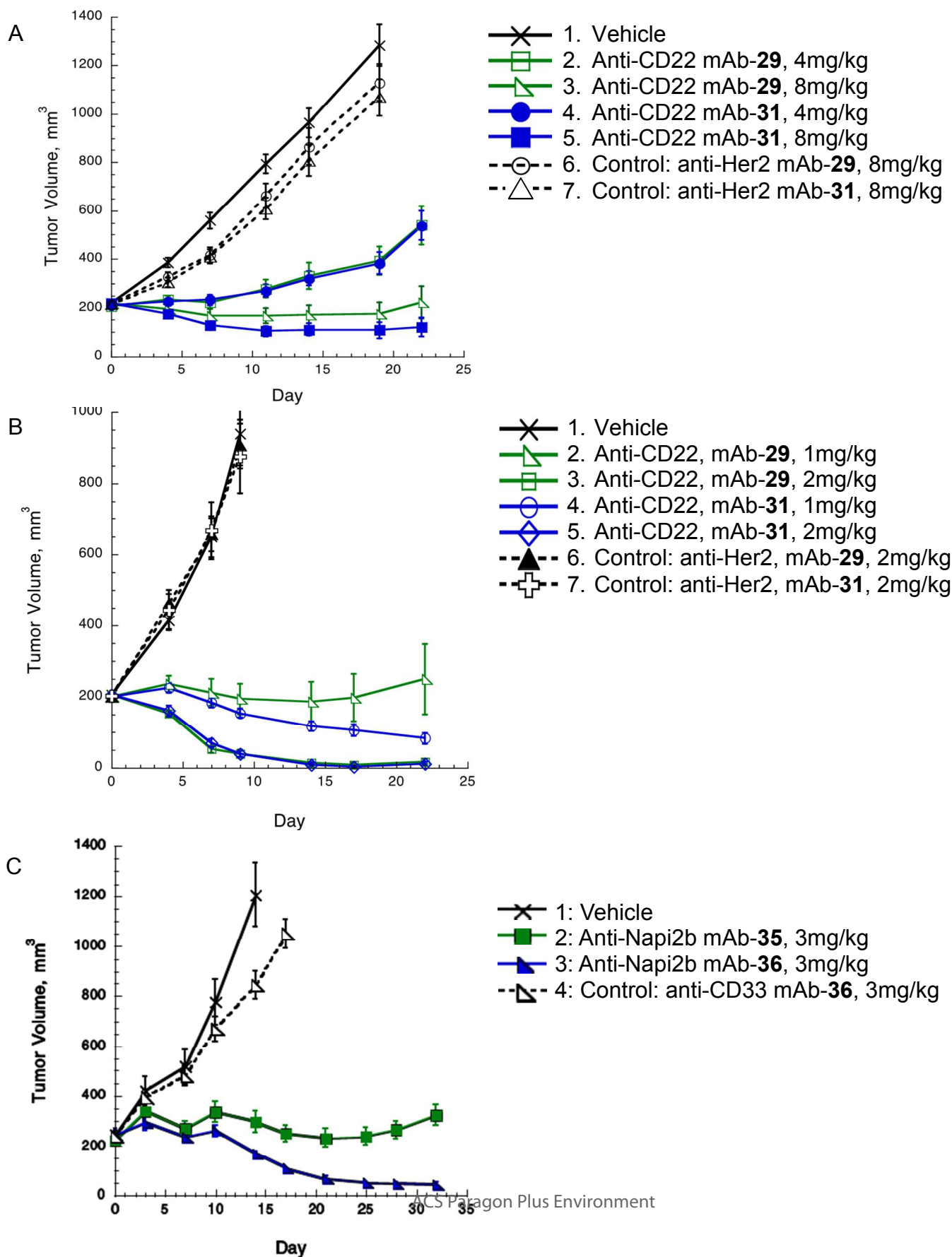


**Figure 6. Comparison of the in vivo stability of ADCs in mice bearing Bjab-luc human lymphoma xenograft.** Blood samples were taken from the mice in group 2 and 4 of the efficacy study shown in Figure 5b, at 1, 7 and 14 days post dosing. A. total antibody concentrations. B. conjugated antibody concentrations.

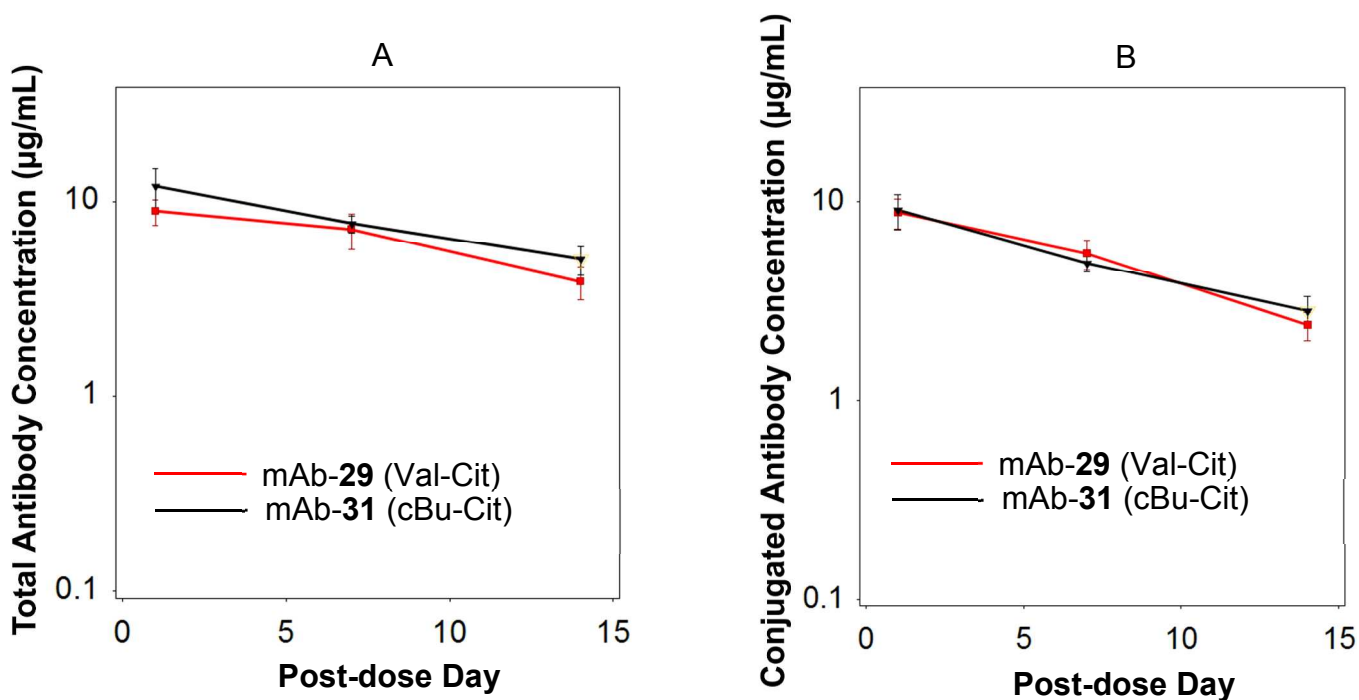


## Table of Contents graphic

